Monthly Notices of the ROYAL ASTRONOMICAL SOCIETY

MNRAS **513,** 4341–4360 (2022) https://doi.org/10.1093/mnras/stac957
Advance Access publication 2022 April 7

Six new compact triply eclipsing triples found with *TESS*

S. A. Rappaport [1]★ T. Borkovits [2,3,4,5]★ R. Gagliano [6] T. L. Jacobs [7] V. B. Kostov [8,9] B. P. Powell [8] I. Terentev [10] M. Omohundro,[10] G. Torres [11] A. Vanderburg [1] T. Mitnyan [2,12] M. H. Kristiansen [13,14] D. LaCourse [15] H. M. Schwengeler [10] T. G. Kaye [16] A. Pál [3,17] T. Pribulla [18] I. B. Bíró [2] I. Csányi,[2] Z. Garai [4,5,18] P. Zasche [19] P. F. L. Maxted [20] J. E. Rodriguez [21] and D. J. Stevens [22,23]

Affiliations are listed at the end of the paper

Accepted 2022 April 1. Received 2022 March 31; in original form 2022 February 23

ABSTRACT

In this work, we report the discovery and analysis of six new compact triply eclipsing triple star systems found with the *TESS* mission: TICs 37743815, 42565581, 54060695, 178010808, 242132789, and 456194776. All of these exhibit distinct third-body eclipses where the inner eclipsing binary (EB) occults the third ('tertiary') star, or vice versa. We utilized the *TESS* photometry, archival photometric data, and available archival spectral energy distribution curves (SED) to solve for the properties of all three stars, as well as many of the orbital elements. We describe in detail our SED fits, search of the archival data for the outer orbital period, and the final global photodynamical analyses. From these analyses, we find that all six systems are coplanar to within $0^\circ - 5^\circ$, and are viewed nearly edge on (i.e. within a couple of degrees). The outer orbital periods and eccentricities of the six systems are $\{P_{\rm out}$ (days), $e\}$: {68.7, 0.36}, {123, 0.16}, {60.7, 0.01}, {69.0, 0.29}, {41.5, 0.01}, {93.9, 0.29}, respectively, in the order the sources are listed above. The masses of all 12 EB stars were in the range of 0.7–1.8 $M_\odot$ and were situated near the main sequence. By contrast, the masses and radii of the tertiary stars ranged from 1.5 to 2.3 $M_\odot$ and 2.9 to 12 $R_\odot$, respectively. We use this information to estimate the occurrence rate of compact flat triple systems..

Key words: binaries: close – binaries: eclipsing – stars: individual: TIC 37743815, TIC 42565581, TIC 54060695, TIC 178010808, TIC 242132789, TIC 456194776.

1 INTRODUCTION

With the advent of long-term, wide field, precision photometry from space with such missions as *Kepler* (Borucki et al. 2010), *K2* (Howell et al. 2014), and *TESS* (Ricker et al. 2015), it has become relatively easy to discover triply eclipsing triple star systems. These are often found when an extra, isolated pair of eclipses appear in the light curve of an ordinary eclipsing binary (EB), or a long exotic-looking extra eclipse appears that cannot be produced in a simple binary (see the recent extensive review of Borkovits 2022). We refer to these as 'third-body' events where either the EB occults the third star (hereafter, the 'tertiary') in its outer orbit, or vice versa. Typical eclipse periods for the inner EBs are days, while the periods for the extra third-body eclipses range from a month to about a year. When one of these triples is found, no further vetting of the object is typically needed before concluding that this is a bound triple system (or possibly a higher stellar multiple). By contrast, when a pair of EBs is found in the same photometric aperture, it is not immediately clear whether the two EBs are physically bound or are simply close together on the sky by chance (see the quadruples catalogue of Kostov et al. 2022), and further vetting in the form of, e.g. radial velocity (RVs) measurements or eclipse timing variations (ETVs) is required.

Once a compact triple system has been identified via its third-body eclipses, several additional characteristics can quickly become apparent about the system. First, if more than one outer eclipse of the same type[1] are seen in succession, then the outer orbital period of the triple is immediately revealed. If both the primary and secondary outer eclipses are seen, then, just as in an ordinary EB, the quantity $e_{\rm out}\cos\omega_{\rm out}$ can be measured, where $e_{\rm out}$ and $\omega_{\rm out}$ are the eccentricity and argument of periastron of the outer orbit, respectively. Finally, the presence of both inner and outer eclipses gives some good indication that the binary orbital plane and the outer orbital plane are at least somewhat aligned (i.e. the systems tend to be 'flat') or else the likelihood of detecting both sets of eclipses is relatively lower.

As we and others have shown in a number of previous papers (see e.g. Carter et al. 2011; Borkovits et al. 2013; Masuda et al. 2015; Orosz 2015; Alonso et al. 2015; Borkovits et al. 2019a, 2020b, 2022), the outer eclipses have encoded in them a substantial amount of information which, when combined with supplementary data, can ultimately lead to a complete description of the stellar properties (masses, radii, $T_{\rm eff}$, age, and metallicity) as well as the complete orbital configuration of the system. The supplemental material can involve the EB light curve itself, the extracted ETV curve, spectral

★ E-mail: sar@mit.edu (SAR); borko@electra.bajaobs.hu (TB)

[1]As in ordinary EBs, outer eclipses come in two flavours – primary and secondary eclipses.

energy distribution (SED) measurements from archival surveys, ground-based photometric surveys, and RVs.

Another feature of compact triple star systems that makes them fascinating objects to study is the relatively short time-scales for dynamical interactions. These can occur over a year, a few months, or even weeks. Interesting effects to look for include dynamical as well as light-traveltime delays in the ETVs of the EBs, forced apsidal motion in the EB, orbital plane precession if the two orbital planes are misaligned, and even large amplitude von Zeipel–Kozai–Lidov cycles (von Zeipel 1910; Kozai 1962; Lidov 1962) in the case of strongly misaligned orbital planes.

Triple star systems are also interesting in terms of the insight they provide about the formation and subsequent evolution of multistellar systems (see e.g. Tokovinin 2021; Borkovits 2022; Section 7). They are the next simplest entity after binary star systems. In some ways, they are analogous to studying He atoms after mastering H atoms. However, while there are more than a million eclipsing binary systems known (see e.g. Section 2; Powell et al. 2021; Kruse et al., in preparation), the number of triply eclipsing triple systems in the literature, is currently under 20.

Here, we present the discovery and detailed analyses of six new compact triply eclipsing triple star systems. In Section 2, we discuss how the discovery of the third-body events was made using the *TESS* data, and present plots of the third-body events. Archival SEDs are then used in Section 3 to make first estimates of the constituent stellar masses, radii, and $T_{\rm eff}$. We then use archival photometric data from a number of ground-based surveys to determine the outer orbital period of the triples via the third-body eclipses (see Section 4). The detailed photodynamical model by which we analyse jointly the photometric light curves, ETVs, and SEDs is reviewed in Section 5. The system parameters for each of the six triple systems are presented in Section 6 in the form of comprehensive tables, including extracted masses, radii, and effective temperatures, as well as the orbital parameters for both the inner and outer orbits. We summarize our results and discuss a few of the salient findings from our study in Section 7. We also discuss how our compact triple systems may inform us about multistellar formation and evolution.

2 DISCOVERY OF TRIPLY ECLIPSING TRIPLES WITH *TESS*

Our 'Visual Survey Group' (VSG; Kristiansen et al. 2022) continues to search for multistellar systems in the *TESS* light curves. We estimate that, thus far, we have visually inspected some 10 million light curves from *TESS*. Such visual searches are a complement to more automated ones using machine learning algorithms (see e.g. Powell et al. 2021; Kostov et al. 2021; Kostov et al. 2022). The light curves are displayed with Allan Schmitt's `LcTools` and `LcViewer` software (Schmitt, Hartman & Kipping 2019), which allows for an inspection of a typical light curve in just ∼5 s. It is important to note that 9 million of the studied light curves were of anonymous stars, while 1 million light curves were of preselected eclipsing binaries that were found in the *TESS* data via machine learning searches (see Powell et al. 2021; Kruse et al., in preparation).

For our survey work, we largely made use of light curves from the following sources: Science Processing Operations Center (SPOC; Jenkins et al. 2016); the Difference Imaging Pipeline (Oelkers & Stassun 2018); the PSF-based Approach to TESS High quality data Of Stellar clusters (PATHOS, Nardiello et al. 2019); the Cluster Difference Imaging Photometric Survey (CDIPS, Bouma, Hartman & Bhatti 2019); the MIT Quick Look Pipeline (QLP, Huang et al. 2020); the TESS Image CAlibrator Full Frame Images (TICA, Fausnaugh et al. 2020); and the Goddard Space Flight Center (GSFC, see section 2 of Powell et al. 2021).

The first signatures that are looked for in terms of identifying triply eclipsing triples are an eclipsing binary light curve with an additional strangely shaped extra eclipse or rapid succession of isolated eclipses. One gratifying aspect of finding triply eclipsing triples is that they are in a sense 'self-vetted'. In particular, there is no way for a single binary, or sets of independent stars or binaries to produce such 'extra' eclipsing events. Therefore, additional vetting becomes largely unnecessary in proving that these are indeed triples (or possibly higher order multiples).

While searching through the light curves obtained from the first three full years of *TESS* observations we have found more than ∼50 of these triply eclipsing triples. Of these we have determined the outer orbital period for 20 of them. We have previously reported on four of these systems (Borkovits et al. 2020b; Borkovits et al. 2022). Here, we present the discovery and analysis of six new triply eclipsing triples from among this set: TIC 37743815, TIC 4256558, TIC 54060695, TIC 178010808, TIC 242132789, and TIC 456194776 (see Table 1 for the main catalogue data of the targets).

All six targets were measured in full frame images from *TESS* with either 30-min or 10-min cadence. A portion of the *TESS* light curves for all six sources are shown in Fig. 1. The sectors during which these sources were observed with *TESS* are summarized in Table 2. TICs 37743815, 42565581, 178010808, and 242132789 were observed during two widely separated sectors each, and a third-body event was observed for each source in both sectors, except for TIC 178010808, for which only one third-body event was detected. TIC 456194776 was observed in only one sector. Finally, TIC 54060695 was observed during three sectors, with a third-body event detected in each – two secondary and one primary outer eclipses.

Given that the sectors are only approximately a month long and the outer orbital periods range from 42 to 123 d, it is somewhat fortuitous that we managed to observe third-body events in nearly all the sectors. However, most of these systems exhibit two eclipses per outer orbit, and we have selected these for presentation in this work precisely because the outer periods are relatively short and therefore easy to detect even in archival data sets. In other words, there are several selection effects at work here.

3 PRELIMINARY SED ANALYSIS

Once we have discovered a triply eclipsing triple, we would like to develop some initial estimates of the nature of the three stars in the system. To do this, we make use of an analysis of the SED. We utilize the VizieR (Ochsenbein, Bauer & Marcout 2000; A.-C. Simon & T. Boch: http://vizier.unistra.fr/vizier/sed/) SED service which, in turn, utilizes systematic sky coverage of such surveys as Skymapper (Wolf et al. 2018), Pan-STARRS (Chambers et al. 2016), SDSS (Gunn et al. 1998), 2MASS (Skrutskie et al. 2006), WISE (Cutri et al. 2013), and in some cases Galex (Bianchi, Shiao & Thilker 2017). These typically provide ∼20 fluxes over the range of 0.35–21 μm.

Unless we have specific information to the contrary, we assume for our preliminary analysis that the three stars in the system have evolved in a coeval fashion since their birth as a triple system. We further assume that there has been no mass transfer among the three stars, in particular between the binary components. Under these assumptions, there are only four parameters that need to be fitted via a Markov chain Monte Carlo approach (see e.g. Ford 2005; Rappaport et al. 2021): $M_{\rm Aa}$, $M_{\rm Ab}$, $M_{\rm B}$, and the age of the system, where *Aa* and *Ab* refer to the stars in the inner binary, while *B* is the tertiary star in the outer orbit. We also make use of *MIST* stellar evolution

Table 1. Main properties of the six triple systems from different catalogues.

Parameter	TIC 37743815	TIC 42565581	TIC 54060695	TIC 178010808	TIC 242132789	TIC 456194776
RA (J2000)	06: 15: 28.89	06: 26: 37.58	06: 56: 14.83	07: 33: 05.27	06: 14: 26.95	03: 28: 29.41
Dec. (J2000)	−29: 39: 12.14	−03: 23: 50.66	−25: 25: 14.49	−04: 23: 20.36	−04: 08: 12.48	43: 36: 44.56
T^a	12.928 ± 0.007	12.867 ± 0.014	12.132 ± 0.022	12.132 ± 0.007	12.636 ± 0.009	11.766 ± 0.008
G^b	13.479 ± 0.001	13.433 ± 0.001	12.679 ± 0.001	12.531 ± 0.000	13.492 ± 0.001	12.243 ± 0.001
$G^b_{\rm BP}$	13.939 ± 0.003	13.955 ± 0.005	13.123 ± 0.003	12.837 ± 0.001	14.325 ± 0.004	12.620 ± 0.002
$G^b_{\rm RP}$	12.859 ± 0.002	12.748 ± 0.002	12.060 ± 0.002	12.062 ± 0.001	12.582 ± 0.003	11.690 ± 0.001
B^a	14.639 ± 0.035	14.626 ± 0.044	13.755 ± 0.112	13.320 ± 0.071	15.454 ± 0.073	12.801 ± 0.396
V^c	13.767 ± 0.126	14.010 ± 0.183	12.884 ± 0.080	12.649 ± 0.069	13.869 ± 0.103	11.997 ± 0.029
J^d	12.075 ± 0.023	11.794 ± 0.023	11.254 ± 0.023	11.544 ± 0.024	11.211 ± 0.021	11.069 ± 0.025
H^d	11.664 ± 0.027	11.335 ± 0.025	10.836 ± 0.023	11.305 ± 0.025	10.560 ± 0.023	10.777 ± 0.029
K^d	11.527 ± 0.021	11.158 ± 0.021	10.735 ± 0.023	11.224 ± 0.025	10.347 ± 0.022	10.705 ± 0.022
$W1^e$	11.476 ± 0.023	11.102 ± 0.023	10.661 ± 0.023	11.221 ± 0.023	10.223 ± 0.022	10.644 ± 0.023
$W2^e$	11.497 ± 0.021	11.149 ± 0.020	10.706 ± 0.020	11.241 ± 0.021	10.259 ± 0.020	10.647 ± 0.021
$W3^e$	11.463 ± 0.149	11.266 ± 0.131	10.597 ± 0.087	11.247 ± 0.140	10.270 ± 0.089	10.617 ± 0.099
$T_{\rm eff}$ (K)^b	5039 ± 100	4895 ± 175	5029 ± 220	5862 ± 30	4015 ± 135	5375 ± 550
$T_{\rm eff}$ (K)^a	5135 ± 125	5374 ± 135	5660 ± 125	6090 ± 126	4593 ± 123	6690 ± 62
R ($R_\odot$)^b	4.73 ± 0.18	8.43 ± 0.60	8.96 ± 0.68	4.12 ± 0.04	14.5 ± 0.9	7.06 ± 1.30
R ($R_\odot$)^a	4.46 ± *NA*	7.97 ± *NA*	7.79 ± *NA*	3.85 ± 0.28	13.3 ± *NA*	5.14 ± *NA*
Distance (pc)^f	1857 ± 39	3281 ± 160	2221 ± 50	1464 ± 30	3258 ± 165	1590 ± 40
$E(B-V)^a$	0.036 ± 0.006	0.213 ± 0.017	0.168 ± 0.033	0.046 ± 0.006	0.336 ± 0.011	0.167 ± *NA*
μ_α (mas yr^{-1})^b	−0.13 ± 0.01	+0.81 ± 0.02	−2.32 ± 0.01	−2.03 ± 0.01	0.63 ± 0.02	−0.18 ± 0.02
μ_δ (mas yr^{-1})^b	+7.58 ± 0.01	−1.03 ± 0.02	+3.26 ± 0.01	−1.17 ± 0.01	−1.31 ± 0.02	−2.74 ± 0.01

Notes. [a]*TESS* Input Catalog (TIC v8.2) (Paegert et al. 2021). [b]*Gaia* EDR3 (Gaia collaboration 2021); the uncertainty in $T_{\rm eff}$ and R listed here is 1.5 times the geometric mean of the upper and lower error bars cited in DR2. [c]AAVSO Photometric All Sky Survey (APASS) DR9, (Henden et al. 2015), http://vizier.u-strasbg.fr/viz-bin/VizieR?-source = II/336/apass9. [d]2MASS catalogue (Skrutskie et al. 2006). [e]*WISE* point source catalogue (Cutri et al. 2013). [f]Bailer-Jones et al. (2021).

tracks (Paxton et al. 2011; Paxton et al. 2015; Paxton et al. 2019; Dotter 2016; Choi et al. 2016) for an assumed solar composition,[2] as well as stellar atmosphere models from (Castelli & Kurucz 2003). If these four parameters can be determined, then the evolution tracks simultaneously determine the stellar radii and effective temperature of all three stars.

In order to fit an SED, one typically requires an accurate distance to the source and the corresponding interstellar extinction, A_V. Since *Gaia* (Gaia collaboration 2021) provides a secure distance with typically better than 5 per cent accuracy, and we can find information on the extinction from a variety of sources (e.g. Bayestar19; Green et al. 2019), in principle we do not need to fit for these parameters. However, we usually add these two quantities to the fitted MCMC parameters, but with priors limited to just ± 4 times the listed uncertainties on them.

In spite of having some 20 SED data points to work with, and only 4–6 free parameters to fit for, this is most often quite insufficient for a decent solution. The reasons are that (i) many of the SED points are sufficiently close to each other in wavelength so that they are not really independent, and (ii) a typical SED curve contains essentially only 4 or 5 defining characteristics, e.g. flux at any given wavelength on the Rayleigh–Jeans tail, wavelength of the peak in the SED curve, sharpness of the falloff at short wavelengths, etc. Therefore, we find it extremely helpful to add a few supplementary constraints in the MCMC fit. These include estimates of the radius and $T_{\rm eff}$ of the tertiary and the ratio $T_{\rm eff,\,Aa}/T_{\rm eff,\,Ab}$. Because all of the tertiary stars in this work are giants,[3] they tend to dominate the light from the system. Therefore, we make use of the *Gaia* DR2 and *TESS* Input Catalogue (TIC v8.2) estimates of the radius and $T_{\rm eff}$ of the 'composite' system measured as a single object (see Table 1). However, because those estimates are hardly a perfect representation of the tertiary, i.e. there are two other stars in the system, though of considerably lower luminosity, we take uncertainties on $T_{\rm eff}$ to be ±300 K and on R_B to be ±2 $R_\odot$. Finally, the temperature ratio of the two EB stars can be estimated approximately from the ratio of their eclipse depths.

Using only this limited information, we fit the SED for all the properties of the stars in our six systems. The results are shown in Fig. 2. In each case, the measured SED points (orange circles) have been corrected for interstellar extinction. The continuous green curves represent the model fits for the stars in the EB, while the cyan curve is for the tertiary. The heavier black curve is the total flux from all three stars. One can get a very good sense from these plots just how much the tertiary dominates the system light. We list on the plots only the nominal best-fitting values for M, R, and $T_{\rm eff}$ for each of the three stars. We do not list the corresponding uncertainties on these parameters here because we employ a more comprehensive photodynamical analysis in Section 5 which utilizes the EB and third-body eclipse contributions to the light curve, as well as the SED, to determine the final and more accurate stellar parameters. None the less, these first estimates of the stellar parameters provide a very quick estimate of what kinds of stars we are dealing with. The formal uncertainties on the masses are typically 10 per cent. These parameters can then be utilized as the initial input guesses to the photodynamical analysis.

We utilize the system parameters for the stars found from this preliminary SED analysis to show in Fig. 3 the locations of the stars superposed on the `MIST` evolution tracks. The tertiaries range from ∼3 to 15 $R_\odot$, with $T_{\rm eff}$ ranging from 6000 K to 4500 K, respectively. By contrast, most of the binary stars are still on the main sequence, and,

[2]Adopted for this preliminary analysis only. See Section 5 for a description of the full, and more general, photodynamical analysis.

[3]The least evolved tertiary is the one in TIC 178010808, a 1.6 $M_\odot$ star of radius 2.9 $R_\odot$ whose luminosity exceeds that of the combined EB stars by nearly a factor of 2.

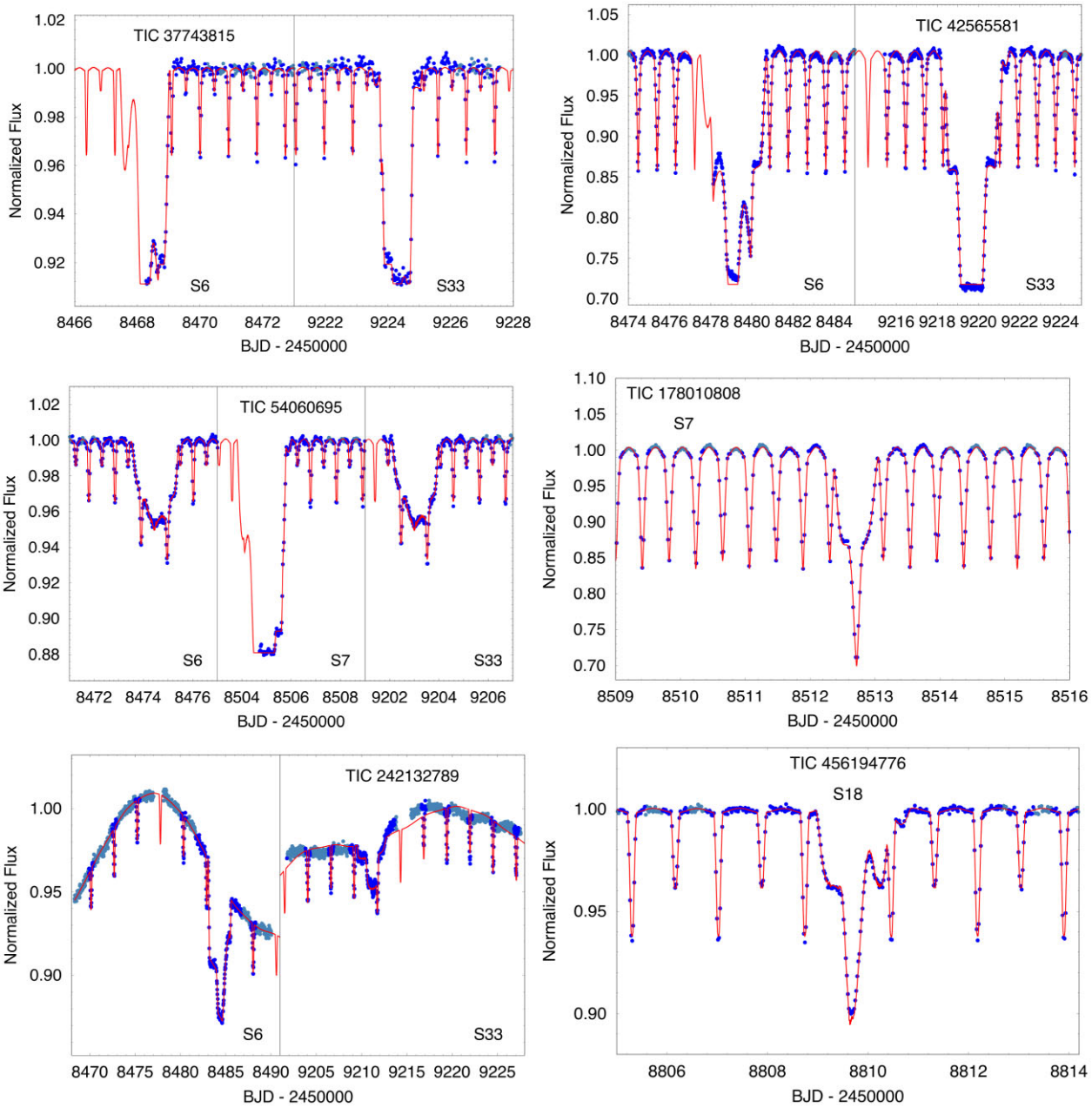

Figure 1. *TESS* third-body light curves. We present a portion of a sector's light curve for each source containing the third-body event that led to their discoveries. For two of the sources there is only a single third-body event that was detected, while in the other four cases we show portions of two or three orbits which exhibited third-body events. The overplotted model light curves are discussed in Section 5. The lighter blue points in the out-of-eclipse region were omitted from the photodynamical fits to save computation time.

Table 2. *TESS* observation sectors for the triples.

Object	Sectors observed	Third-body events
TIC 37743815	S6 & S33	S6 & S33
TIC 42565581	S6 & S33	S6 & S33
TIC 54060695	S6 & S7 & S33	S6 & S7 & S33
TIC 178010808	S7 & S34	S7
TIC 242132789	S6 & S33	S6 & S33
TIC 456194776	S18	S18

with only one exception, range in mass from 1.0 to 1.8 $M_\odot$. Within four of the systems the two EB stars tend to have similar masses.

As a final note on the SED analysis, we point out that we have not considered pre-MS solutions. These are considered and rejected in the photodynamical analysis.

4 OUTER ORBITAL PERIOD DETERMINATION WITH ARCHIVAL DATA

Once we have discovered a triply eclipsing triple system with *TESS*, the most important question to answer after determining the basic parameters of the constituent stars is the nature of its outer orbit,

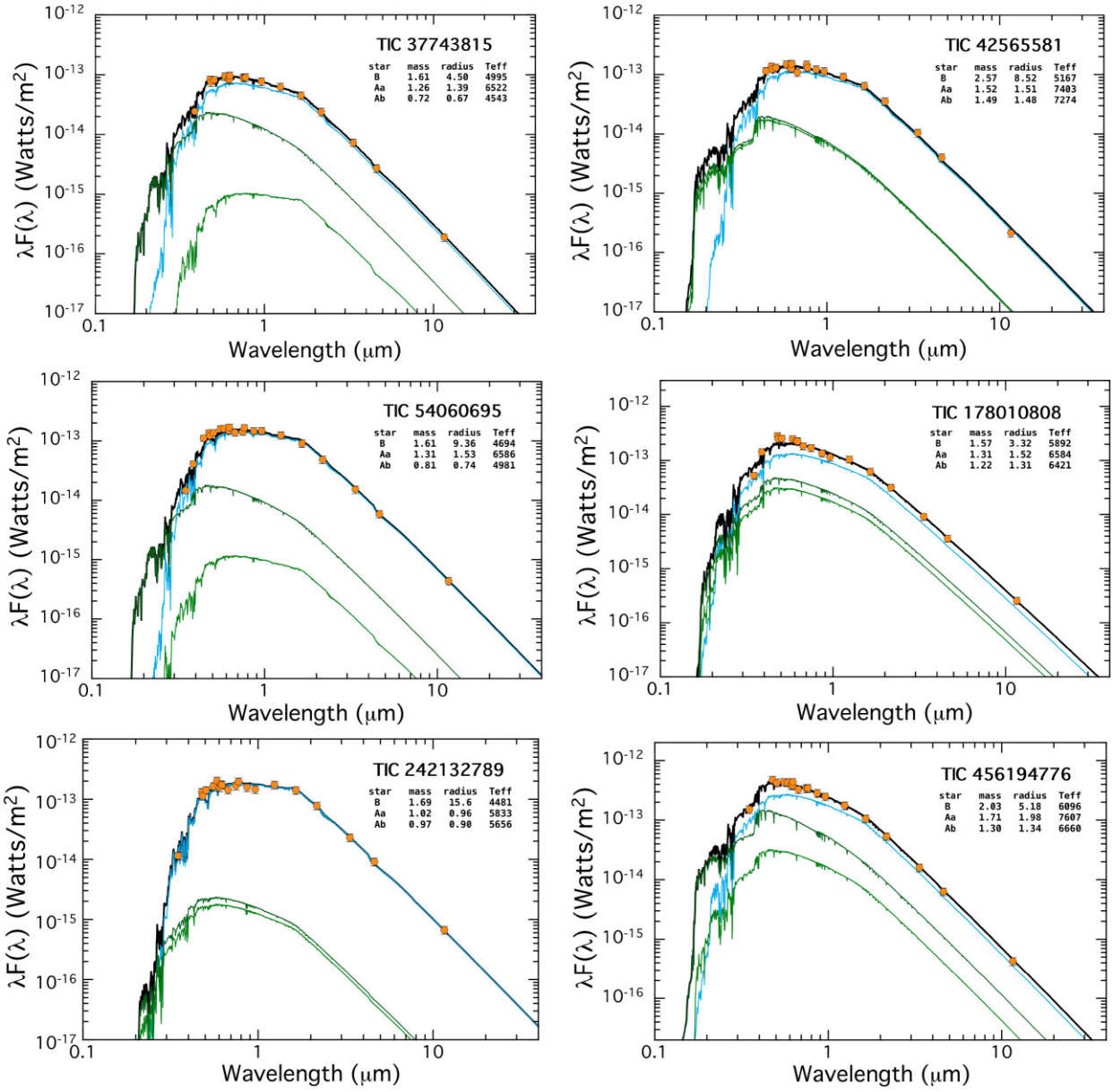

Figure 2. SED fits for each of the six triply eclipsing triples discussed in this work. The cyan curve represents the model spectrum of the tertiary star, (B) while the green curves represent the EB stars (Aa and Ab). The black curve is the sum of the three model spectra. The fits for the three stellar masses, radii, and $T_{\rm eff}$'s were made using only the ∼20 measured SED points, a very loose constraint on the radius and $T_{\rm eff}$ for the tertiary star, and a temperature ratio for the inner EB based on eclipse depths (see Section 3 for details). We also explicitly make the assumption that the three stars are evolving in a coeval fashion without mass transfer. The units on the inset tables are $M_\odot$, $R_\odot$, and K. Typical formal uncertainties on the masses are ∼10 per cent.

in particular the period and eccentricity. For this purpose, in the absence of RV data, we most often make use of the ASAS-SN (Shappee et al. 2014; Kochanek et al. 2017) and ATLAS (Tonry et al. 2018; Smith et al. 2020) archival data sets. The ASAS-SN data sets typically have ∼1500–3000 photometric measurements of a given target, while the ATLAS archives often have approximately 1700 photometric measurements. The ATLAS data have the advantage of going somewhat deeper than the ASAS-SN data, but the disadvantage of saturating on brighter stars where ASAS-SN may still perform well. When these two data sets are of comparable quality, we typically add them. Naturally, we also check for KELT (Pepper et al. 2007, 2012), WASP (Pollacco et al. 2006), HAT (Bakos et al. 2002), and MASCARA data (Talens et al. 2017) to see whether they are available for a particular source.

For all the sources, with the exception of TIC 242132789, there were WASP archival data available. We found these to be quite useful in helping to determine the long-term average EB periods. But, it turns out that these data were generally too noisy to aid in the search for the outer third-body eclipses, except in the case of TIC 178010808 where the WASP data nicely complemented the ATLAS and ASAS-SN data. For TIC 242132789 there was a set of KELT data in addition to ATLAS and ASAS-SN data. The KELT data marginally detected the spot and ellipsoidal light modulations associated with the outer orbit, but not the outer eclipses.

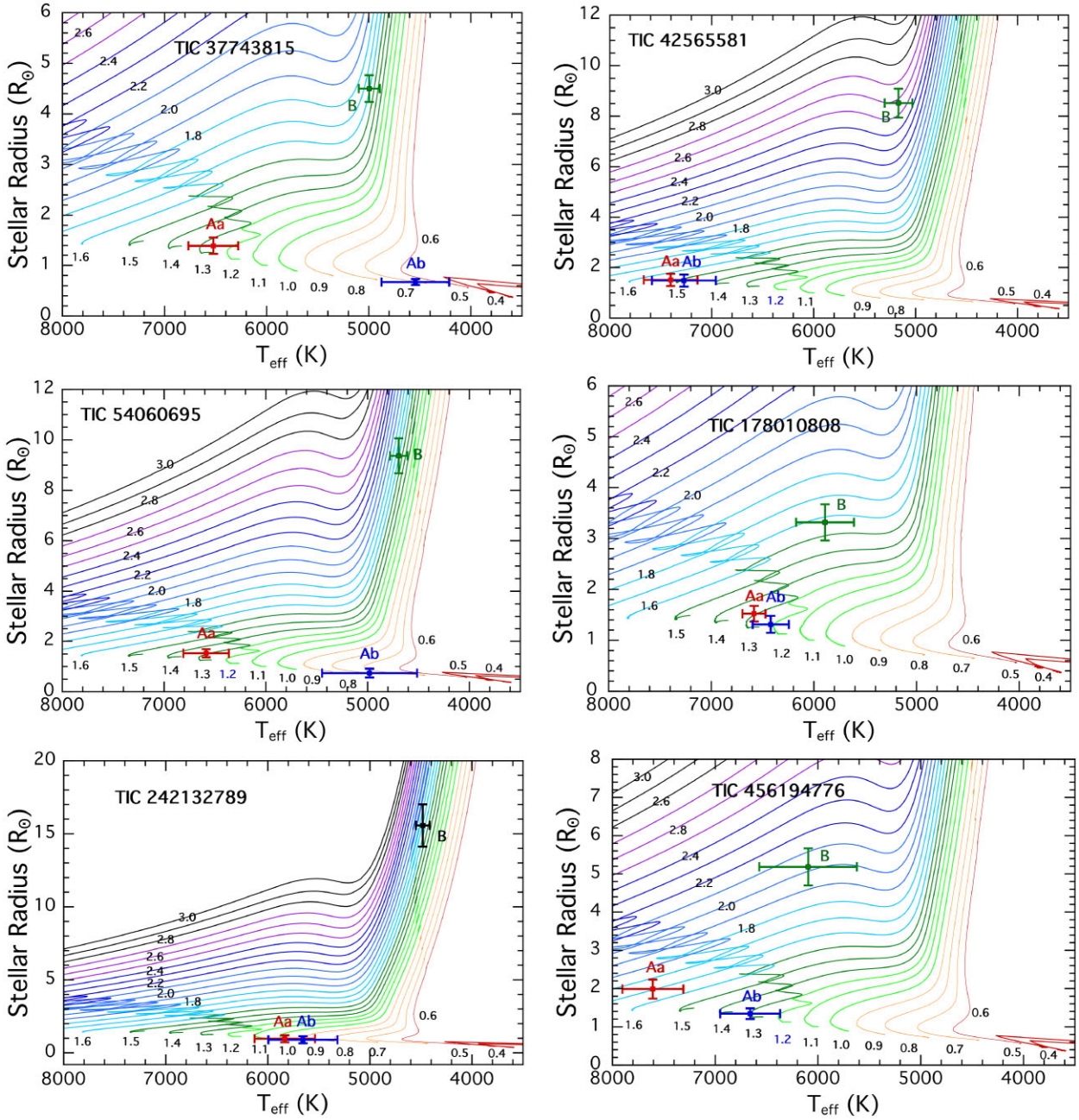

Figure 3. The locations of the three stars in each of the six triple systems shown superposed on the MIST stellar evolution tracks for stars of solar composition. The numbers next to the tracks are the stellar masses in $M_\odot$. The locations of the stars in this diagram were taken from the SED fits shown in Fig. 2. Somewhat more accurate stellar parameters are tabulated in Section 5 based on the full photodynamical analyses. However, the locations do not generally move appreciably (see Section 6.1).

We do a blind search for the outer eclipses (either outer primary or outer secondary eclipse) using a Box Least Squares transform (Kovács, Zucker & Mazeh 2002). Before doing the BLS search we remove the light curve of the inner EB by Fourier means (as described in Powell et al. 2021). In the process, we remove between 5 and 100 orbital harmonics depending on the sharpness of the features in the EB light curve. This cleaning process requires knowing the orbital period of the EB very accurately. In turn, we determine the long-term average binary period from the *TESS* data or from the archival data, whichever yield a more precise result.

We show the results of the above procedure for each of our six triply eclipsing triple stars in Fig. 4. In each panel, we show a folded, binned, and averaged light curve of the archival data about the period corresponding to the largest and most significant peak in the BLS transform. In all cases, the zero phase for the outer orbit is taken to be the time of one of the third-body eclipses observed in the *TESS* data. In four of the six sources, both the primary and secondary outer eclipses are clearly detected. In those cases, the value of $e\cos\omega_{\rm out}$ is also accurately determined, in addition to the outer period of the triple. In the fifth source, TIC 178010808, the secondary outer eclipse is only barely detected, if at all. In the sixth source,

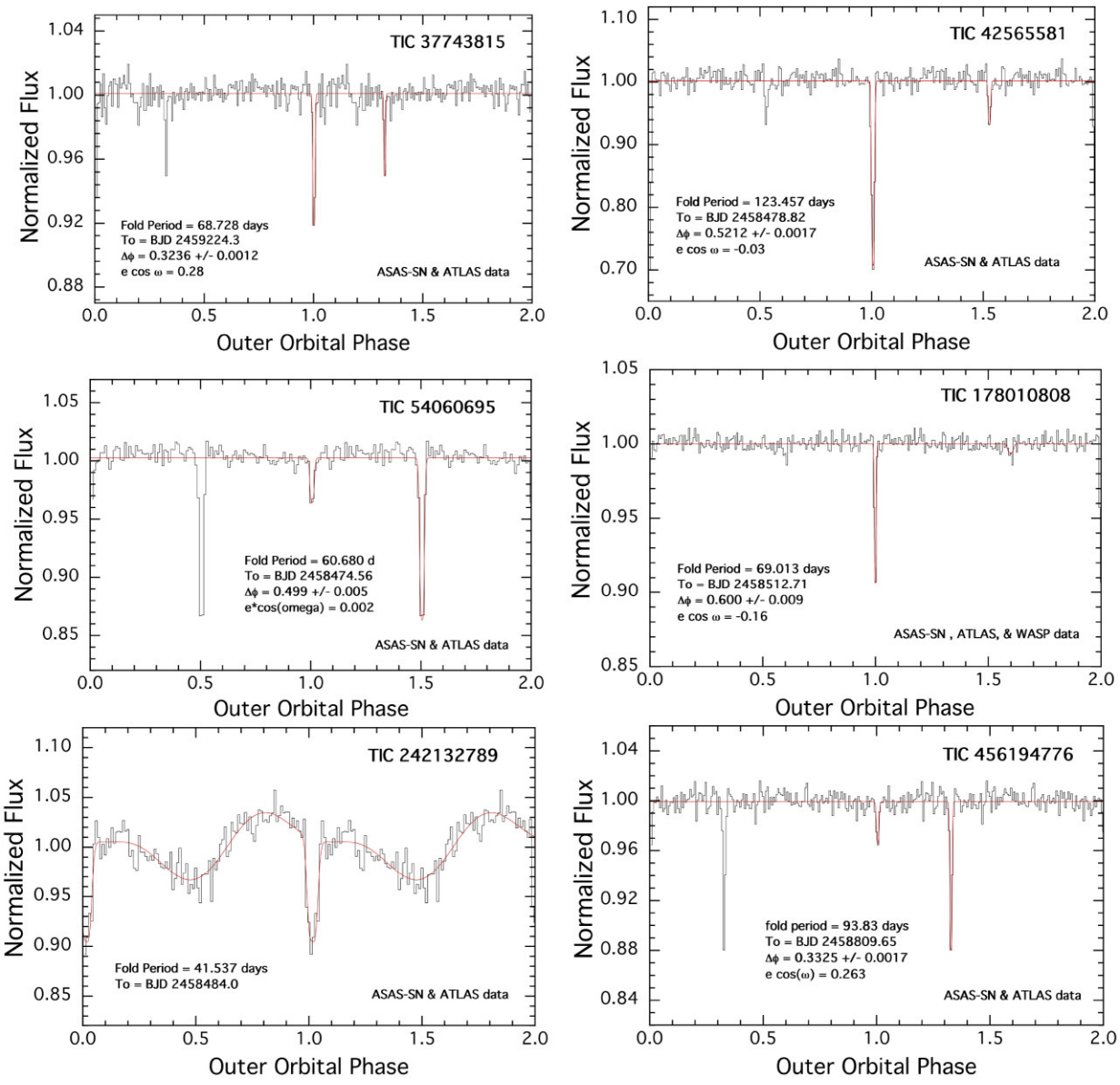

Figure 4. Folded, binned, and averaged light curves for the outer orbits of the six triply eclipsing triple stars. These are based on archival data from ATLAS, ASAS-SN, and WASP data (see Section 4 for details). On each plot, we write the fold period, the epoch reference time of phase zero, the orbital phase difference between the primary and secondary outer eclipses (if both are detected), and the inferred value of $e\cos\omega_{\rm out}$ based on the fold. The red curve is a fit to the one or two outer eclipses during the second plotted orbital cycle only. These are used to measure the orbital phase difference between the two eclipses and the widths (where possible and appropriate).

TIC 242132789, the outer orbital light curve has a clear undulating structure superposed on the very clear primary eclipse. Because the slow modulations have the same period as the outer eclipses, we attribute this to starspot(s) on a giant tertiary that is corotating with the binary orbit as well as to ellipsoidal light variations from the giant. Note that the giant in this system has $R \simeq 15\,{\rm R}_\odot$. Not only is this star large, but its outer orbital period of 42 d is the shortest among our sample, and one of the shortest period triples known.

5 PHOTODYNAMICAL ANALYSIS FOR THE SYSTEM PARAMETERS

For all six of our triply eclipsing triples, we have carried out a photodynamical analysis with the software package LIGHTCURVEFACTORY (see e.g. Borkovits et al. 2019a, 2020a, and references therein). As described in earlier work, the code contains (i) a built-in numerical integrator to calculate the three-body perturbed coordinates and velocities of the three stars in the system; (ii) emulators for the *TESS* light curve, the ETVs extracted therefrom, and radial velocity curve (if available), and (iii) an MCMC-based search routine for the system parameters. The latter utilizes an implementation of the generic Metropolis-Hastings algorithm (see e.g. Ford 2005). The use of this software package and the consecutive steps of the entire analysis process have been previously explained in detail as the code was applied to a wide range of multistellar systems (Borkovits et al. 2018, 2019a,b, 2020a,b, 2021; Mitnyan et al. 2020). These included tight and wider triple systems (with and without outer eclipses), as well as quadruple systems with either a 2+2 or 2+1 + 1

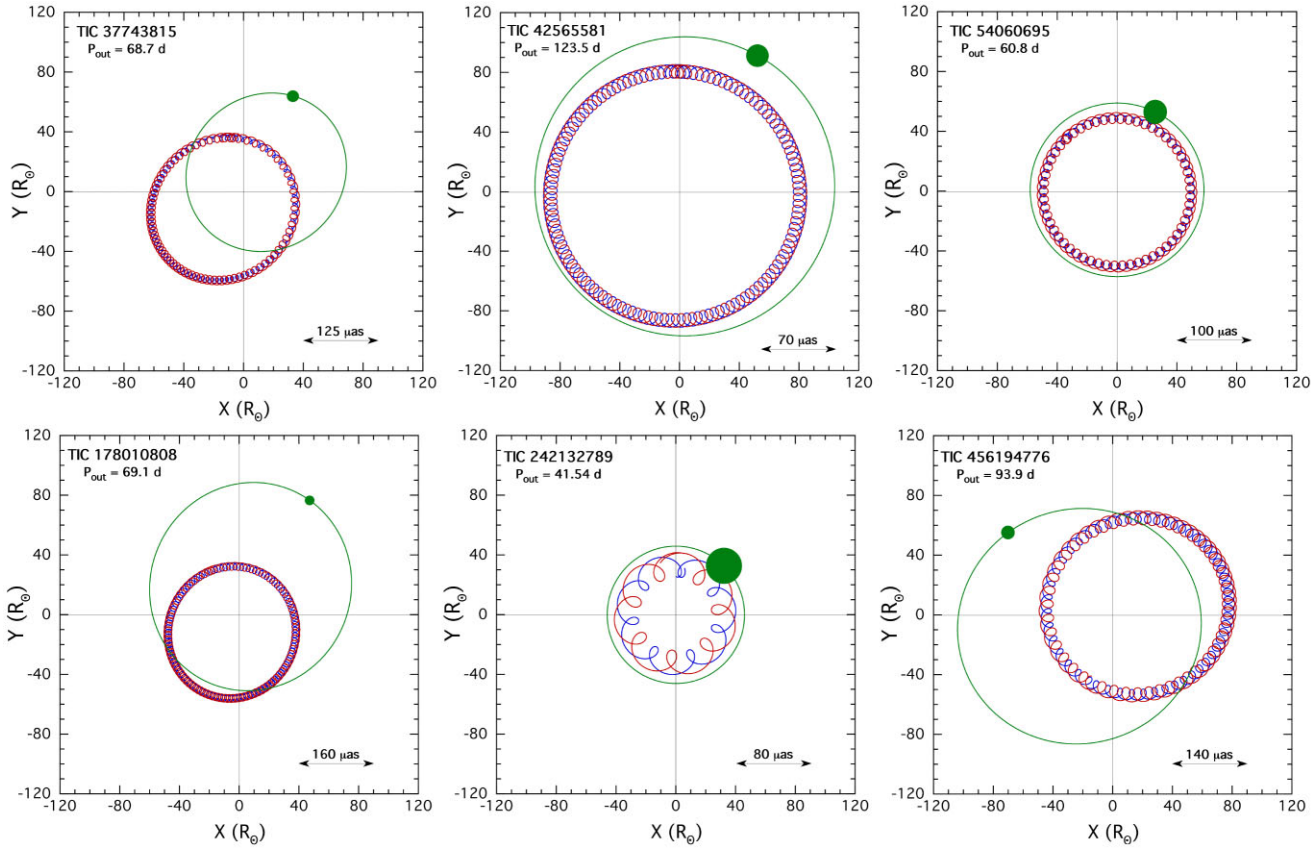

Figure 5. The outer orbits of the six triply eclipsing systems seen from above the orbital plane. The stars are all moving counterclockwise. The observer is at $y \rightarrow -\infty$. Red and blue tracks are for the primary and secondary stars in the EB, respectively, while the green track is that of the tertiary star. The heavy filled green circle represents the size of the tertiary to scale on the plot. Each panel has an angular scale in units of micro-arcseconds. A discussion about how the stellar motions may affect the *Gaia* distance determinations is given in Appendix C.

configuration. Here, we discuss only a few specific points related to the current triples.

In relatively close systems, as we are studying here, perturbations to the EB orbit and the detailed profiles of the third-body eclipses carry important information about the system parameters, including constraints on the masses and orbital elements. However, with only one exception in this current work, we have no RV measurements to help constrain the system parameters. Therefore, we adopt a somewhat different strategy. In the analysis we utilize some a priori knowledge of stellar astrophysics and evolution with the use of PARSEC isochrones and evolutionary tracks (Bressan et al. 2012). We make use of tabulated three-dimensional grids in triplets of {age, metallicity, initial stellar mass} of PARSEC isochrones that have stellar temperatures, radii, surface gravities, luminosities, and magnitudes in different passbands of several photometric systems. Then, we allow the three parameters {age, metallicity, initial stellar mass} to vary as adjustable MCMC variables. The stellar temperature, radius, and actual passband magnitude are calculated through trilinear interpolations from the grid points and these values are used to generate synthetic light curves and an SED that can be compared to their observational counterparts. This process, which is also built into LIGHTCURVEFACTORY, is described in detail in Borkovits et al. (2020a). In our prior work, we have termed these solutions 'MDN' (model-dependent-no-RV solutions) which is what we implement here.

Regarding the technical details, in the case of the stellar evolution model dependent runs, the freely adjusted (i.e. trial) parameters were as follows:

(i) Stars: Three stellar masses and the 'extra light' contamination, ℓ_4, from a possible fourth star (or any other contaminating sources in the *TESS* aperture). Additionally, the metallicity of the system ([*M*/*H*]), the (logarithmic) age of the three stars ($\log \tau$), the interstellar reddening $E(B-V)$ towards the given triple, and its distance, were also varied.

(ii) Orbits: Three of six orbital-element related parameters of the inner, and six parameters of the outer orbits, i.e. the components of the eccentricity vectors of the two orbits $(e\sin\omega)_{\rm in,\,out}$, $(e\cos\omega)_{\rm in,\,out}$, the inclinations relative to the plane of the sky ($i_{\rm in,\,out}$), and moreover, three other parameters for the outer orbit, including the period ($P_{\rm out}$), time of the first (inferior or superior) conjunction of the tertiary star observed in the *TESS* data ($\mathcal{T}_{\rm out}^{\rm inf,sup}$) and, finally, the longitude of the node relative to the inner binary's node ($\Omega_{\rm out}$).

Here, we add some additional notes about the 'age' and the 'distance'. First, regarding the 'age' parameter, our previous experience has led us to believe that, in some cases, it is better to allow the ages of the three stars to be adjusted individually instead of requiring strict coeval evolution. This issue was briefly discussed in Rowden et al. (2020) and Borkovits et al. (2021), and we discuss it below in the case of some individual sources. Regarding the distance of the triple system, one can argue that the accurate trigonometric

distances obtained with *Gaia* (Bailer-Jones et al. 2021) should be used as Gaussian priors to penalize the model solutions. But, given that neither DR2 nor the recently released eDR3 *Gaia* parallaxes have been corrected for the multistellar nature of the objects, we consider the published parallaxes and corresponding distances to be not necessarily accurate for our systems. Therefore, we decided not to utilize the *Gaia* distances. Instead, we constrained the distance by minimizing the $\chi^2_{\rm SED}$ value a posteriori, at the end of each trial step (for results see Section 6.1).

A couple of other parameters were *constrained* instead of being adjusted or held constant during our analyses. Specifically, the orbital period of the inner binary ($P_{\rm in}$) and its orbital phase (through the time of an arbitrary primary eclipse or, more strictly, the time of the inferior conjunction of the secondary star – $\mathcal{T}_{\rm in}^{\rm inf}$) are in this category. They were constrained internally through the ETV curves.

Regarding the atmospheric parameters of the stars, we handled them in a similar manner as in our previous photodynamical studies. We utilized a logarithmic limb-darkening law (Klinglesmith & Sobieski 1970) for which the passband-dependent linear and non-linear coefficients were interpolated in each trial step via the tables from the original version of the `Phoebe` software (Prša & Zwitter 2005). We set the gravity darkening exponents for all late type stars to $\beta = 0.32$ in accordance with the classic model of Lucy (1967) valid for convective stars and hold them constant. For several of our systems, however, the analysis of the net SED has revealed that the EBs contain hotter stars, having radiative envelopes. For these stars, we set $\beta = 1.0$. The choice of this parameter, however, has only minor consequences, as the stars under the present investigation are close to spheroids.

For the photodynamical analysis we utilized a more sophisticated processing for the *TESS* photometric data by employing the convolution-based differential image analysis tasks of the FITSH package Pál (2012). Furthermore, we note that in preparing the observational data for analysis, to save computational time we dropped out the out-of-eclipse sections of the 30-min cadence *TESS* light curves, retaining only the $\pm 0\overset{\rm p}{.}15$ phase-domain regions around the binary eclipses themselves. However, during sections of the data containing the third-body (i.e. 'outer') eclipses, we kept the data for an entire binary period both before and after the first and last contacts of the given third-body eclipse.

Moreover, the mid-eclipse times of the inner binaries, used to define the ETV curves, were calculated in a manner that was described in detail in Borkovits et al. (2016). The ETVs were one of the inputs to the photodynamical analysis. We tabulate all the eclipse times in Appendix B as online only tables.

Finally, note also some system-specific departures from the standard procedures described above in the case of two of our triples. These are as follows:

(i) In the case of TIC 242132789, the light curve of both *TESS* sectors display non-linear, somewhat erratic variations in the mean out-of-eclipse flux levels. This can partly be attributed to the ellipsoidal light variations (ELV) of the red giant tertiary, which is handled internally by our light-curve emulator and, therefore, nothing special has to be done to model the ELVs. However, an additional, more erratic contribution to these variations might arise from either time-varying spot activity on the surface of the red giant or any stray light in the aperture (or both). In any case, independent of the origin(s) of this time-varying, irregular contaminating flux, we modelled it by fitting an eighth order polynomial, separately for the two sectors, simultaneously with the triple star light-curve modelling, during each MCMC step.

(ii) The other triple that was handled somewhat differently is TIC 456194776. This system was originally the fourth target of the ground-based photometric follow-up campaign that was described in detail in section 2.3 of Borkovits et al. (2022). In contrast to the other three triply eclipsing triples, of which the detailed analyses were published in Borkovits et al. (2022), unfortunately, we were unable to catch any further third-body eclipses during our observing runs. This is the reason why this system was not included the above-mentioned study, but rather appears in this work. On the other hand, however, we were able to observe nine regular inner eclipses from the ground between 12 August 2020 and 12 December 2021. Thus, we decided to include these eclipsing light curves (in Cousins R_C-band) and also the extracted eclipse times in our analysis. In addition, near the final stages of our analysis we also acquired RV data for this target. Therefore, we carried out a second kind of analysis for this target which we have termed 'MDR' (model-dependent-with-RVs) with the inclusion of these RV points. We discuss this latter, MDR solution and compare it with the MDN results in Appendix A2. This second type of analysis might also be called a 'spectrophotodynamical solution'.

6 STELLAR AND ORBITAL PARAMETERS FOR THE SIX TRIPLES

6.1 Individual triples

In this section, we briefly discuss the results for each of the six triply eclipsing triples. The stellar and orbital parameters for each system are given Tables 3 to 6 and are based on the photodynamical fits. As a quick overview of what the systems 'look like' we show in Fig. 5 a plot (to scale) of the three stellar orbits in each system.

6.1.1 TIC 37743815

The outer period for this system is 68.80 days from the photodynamical solution and 68.72[4] from the BLS transform of the ASAS-SN and ATLAS data sets. The EB period is 0.9071 d. The quantity $e_{\rm out}\cos\omega_{\rm out}$ from a fold of the latter data is 0.28. The photodyamical fit yields $e_{\rm out} = 0.361$ and $\omega_{\rm out} = 40.5^\circ$, which combine to give $e_{\rm out}\cos\omega_{\rm out} = 0.27$, in excellent agreement with the findings of the archival data. The mutual inclination angle between the inner EB and outer orbit is $1.8^\circ \pm 1^\circ$. The overall system is incredibly flat with $i_{\rm in}$ and $i_{\rm out}$ both within $1/2^\circ$ of 90°.

The mass and radius of the tertiary are 1.6 $M_\odot$ and 4.0 $R_\odot$, respectively. Both EB stars are considerably lower in mass at 1.1 $M_\odot$ and 0.7 $M_\odot$. The results from the SED fit (Fig. 2) give the same mass for the tertiary star and a radius that is 12 per cent larger than the photodyamical solution. The primary in the EB has a 16 per cent higher mass from the SED fit than given by the photodynamical fit, while the secondary EB mass is in excellent agreement. In fact, it is instructive to compare the results of the SED fits with those of the more detailed photodyamical results as a type of calibration of the former approach. We mention these comparisons for all the systems.

The distance from the photodynamical fit of 1790 pc is within the uncertainties of 1857 pc given in Table 1. $E(B-V)$ from the photodynamical fit is somewhat higher than the value given in Table 1. We estimate the age of the system as 2.4 Gyr.

[4]In this section, we cite the eclipsing periods, taken from Table 6.

Table 3. Orbital and astrophysical parameters of TIC 37743815 and TIC 42565581 from the joint photodynamical *TESS*, ETV, SED and PARSEC isochrone solution. Note that the orbital parameters are instantaneous, osculating orbital elements and are given for epoch t_0 (first row). Therefore, the orbital periods, in particular, cannot be used for predicting the times of future eclipses; see Table 6 for the latter, and Kostov et al. (2021) for a detailed explanation.

	TIC 37743815		TIC 42565581	
	Orbital elements			
	subsystem		Subsystem	
	Aa–Ab	A–B	Aa–Ab	A–B
t_0 [BJD – 2400000]	58468.0		58468.0	
P [d]	$0.906926^{+0.000008}_{-0.000009}$	$68.7998^{+0.0029}_{-0.0025}$	$1.823537^{+0.000031}_{-0.000035}$	$123.5467^{+0.0041}_{-0.0039}$
a [$R_\odot$]	$4.779^{+0.026}_{-0.037}$	$105.8^{+1.1}_{-0.6}$	$9.61^{+0.12}_{-0.16}$	$187.9^{+3.3}_{-2.8}$
e	$0.0093^{+0.0065}_{-0.0035}$	$0.361^{+0.018}_{-0.016}$	$0.01227^{+0.00041}_{-0.00040}$	$0.161^{+0.107}_{-0.017}$
ω (deg)	$95.0^{+3.6}_{-3.8}$	$40.5^{+2.8}_{-3.6}$	$163.5^{+4.3}_{-3.4}$	64^{+16}_{-28}
i (deg)	$89.55^{+0.53}_{-0.39}$	$89.60^{+0.16}_{-0.56}$	$90.26^{+0.31}_{-0.53}$	$89.10^{+1.35}_{-0.27}$
$\mathcal{T}_0^{\rm inf}$ [BJD – 2400000]	$58469.09761^{+0.00014}_{-0.00004}$	$58468.2849^{+0.0111}_{-0.0096}$	$58468.9993^{+0.0002}_{-0.0002}$	$58479.1476^{+0.0076}_{-0.0096}$
τ [BJD – 2400000]	$58486.6584^{+0.0092}_{-0.0097}$	$58417.24^{+0.47}_{-0.61}$	$58468.469^{+0.022}_{-0.017}$	$58405.4^{+7.4}_{-16.5}$
Ω (deg)	0.0	$-1.08^{+1.92}_{-2.17}$	0.0	$4.72^{+1.59}_{-9.91}$
$i_{\rm m}$ (deg)	$1.84^{+1.49}_{-0.82}$		$5.53^{+1.63}_{-1.69}$	
Mass ratio ($q = m_{\rm sec}/m_{\rm pri}$)	$0.642^{+0.010}_{-0.010}$	$0.905^{+0.017}_{-0.053}$	$0.997^{+0.004}_{-0.004}$	$0.638^{+0.036}_{-0.014}$
$K_{\rm pri}$ (km s^{-1})	$104.3^{+1.1}_{-1.5}$	$39.9^{+0.7}_{-2.2}$	$132.6^{+1.1}_{-1.0}$	$30.6^{+1.3}_{-0.7}$
$K_{\rm sec}$ (km s^{-1})	$162.3^{+1.3}_{-2.5}$	$44.0^{+0.4}_{-0.3}$	$132.9^{+1.2}_{-0.9}$	$47.5^{+1.7}_{-1.0}$
	Stellar parameters			
	Aa	Ab	B	Aa	Ab	B
	Relative quantities					
Fractional radius (R/a)	$0.2201^{+0.0031}_{-0.0039}$	$0.1376^{+0.0008}_{-0.0023}$	$0.0377^{+0.0037}_{-0.0014}$	$0.2382^{+0.0024}_{-0.0025}$	$0.2358^{+0.0026}_{-0.0025}$	$0.0451^{+0.0020}_{-0.0027}$
Temperature relative to $(T_{\rm eff})_{\rm Aa}$	1	$0.7202^{+0.0107}_{-0.0094}$	$0.9244^{+0.0163}_{-0.0362}$	1	$1.0001^{+0.0007}_{-0.0006}$	$0.6959^{+0.0204}_{-0.0133}$
Fractional flux (in *TESS* band)	$0.0804^{+0.0011}_{-0.0011}$	$0.0081^{+0.0006}_{-0.0006}$	$0.8957^{+0.0118}_{-0.0251}$	$0.1417^{+0.0017}_{-0.0016}$	$0.1393^{+0.0015}_{-0.0015}$	$0.6093^{+0.0334}_{-0.0303}$
	Physical quantities					
m ($M_\odot$)	$1.082^{+0.020}_{-0.021}$	$0.697^{+0.012}_{-0.024}$	$1.605^{+0.052}_{-0.085}$	$1.793^{+0.067}_{-0.089}$	$1.787^{+0.068}_{-0.087}$	$2.255^{+0.233}_{-0.113}$
R ($R_\odot$)	$1.052^{+0.020}_{-0.028}$	$0.659^{+0.006}_{-0.017}$	$4.011^{+0.362}_{-0.152}$	$2.288^{+0.034}_{-0.047}$	$2.266^{+0.035}_{-0.047}$	$8.410^{+0.583}_{-0.485}$
$T_{\rm eff}$ (K)	5899^{+94}_{-70}	4255^{+112}_{-85}	5434^{+140}_{-210}	7521^{+117}_{-153}	7521^{+119}_{-155}	5218^{+168}_{-130}
$L_{\rm bol}$ ($L_\odot$)	$1.214^{+0.075}_{-0.082}$	$0.126^{+0.012}_{-0.009}$	$12.79^{+0.60}_{-0.72}$	$15.14^{+0.87}_{-1.61}$	$14.83^{+0.92}_{-1.53}$	$47.74^{+3.77}_{-3.09}$
$M_{\rm bol}$	$4.56^{+0.08}_{-0.07}$	$7.02^{+0.08}_{-0.10}$	$2.00^{+0.06}_{-0.05}$	$1.82^{+0.12}_{-0.06}$	$1.84^{+0.12}_{-0.07}$	$0.57^{+0.07}_{-0.08}$
M_V	$4.59^{+0.08}_{-0.07}$	$7.85^{+0.18}_{-0.20}$	$2.16^{+0.07}_{-0.06}$	$1.76^{+0.14}_{-0.06}$	$1.78^{+0.13}_{-0.07}$	$0.78^{+0.08}_{-0.09}$
$\log g$ (dex)	$4.427^{+0.012}_{-0.009}$	$4.644^{+0.006}_{-0.002}$	$3.438^{+0.036}_{-0.090}$	$3.969^{+0.012}_{-0.010}$	$3.976^{+0.012}_{-0.010}$	$2.935^{+0.057}_{-0.030}$
	Global system parameters					
log (age) (dex)		$9.384^{+0.069}_{-0.021}$			$9.044^{+0.066}_{-0.059}$	$8.935^{+0.027}_{-0.089}$
$[M/H]$ (dex)		$0.140^{+0.122}_{-0.086}$			$0.050^{+0.145}_{-0.176}$	
$E(B-V)$ (mag)		$0.158^{+0.047}_{-0.054}$			$0.392^{+0.051}_{-0.039}$	
Extra light ℓ_4 (in *TESS* band)		$0.016^{+0.025}_{-0.012}$			$0.110^{+0.031}_{-0.034}$	
$(M_V)_{\rm tot}$		$2.04^{+0.07}_{-0.06}$			$0.13^{+0.10}_{-0.06}$	
Distance (pc)		1789^{+112}_{-55}			3150^{+196}_{-117}	

6.1.2 TIC 42565581

The outer orbital period of this triple is the longest among our sample of six systems at 123.5 days. This is in excellent agreement with what we found from the archival photometric data. The EB period is 1.8231 d. The system is not exceptionally flat with $i_{\rm mut} = 5.5^\circ \pm 1.6^\circ$ with the inclination angles of the inner and outer orbits both within a few tenths of a degree of edge on. The eccentricity of the outer orbit is $e_{\rm out} = 0.16$ with $\omega_{\rm out} \simeq 61^{+16}_{-28}$ deg. This combination would be in disagreement with the value of $e_{\rm out}\cos\omega_{\rm out} = 0.03$ found from the archival photometric data unless the former value of $\omega_{\rm out}$ is near its 1σ upper limit of $\sim 77^\circ$.

The tertiary star is the most massive of our sample at 2.2 $M_\odot$, and is substantially evolved off the main sequence with R = 8.4 $R_\odot$. The EB stars are near twins with masses of 1.79 $M_\odot$, which are much hotter at 7500 K than the tertiary at 5200 K. These are all in satisfactory agreement with the results of our simpler SED fit, except that the mass of the tertiary in the latter fit was about 14 per cent higher, while the EB stars were ∼20 per cent lower in mass. The radius of the tertiary was the same in both fits.

We find a photometric distance to this source of 3150 pc (with an uncertainty of ∼150 pc), which agrees with the *Gaia* distance of 3280± 160 pc. The fitted $E(B-V)$ for this source is 0.39 ± 0.04 compared with the literature tabulated value of only 0.21 ± 0.02. Finally, we find an age 0.89 ± 0.12 Gyr for the tertiary versus 1.11 ± 0.15 Gyr for the EB when the two are allowed to have independent ages.

Table 4. The same as in Table 3 above, but for TIC 54060695 and TIC 178010808.

	TIC 54060695		TIC 178010808	
	orbital elements			
	subsystem		subsystem	
	Aa–Ab	A–B	Aa–Ab	A–B
t_0 (BJD – 2400000)	58468.0		58491.5	
P (d)	$1.060801^{+0.000014}_{-0.000017}$	$60.7759^{+0.0011}_{-0.0011}$	$0.826496^{+0.000014}_{-0.000014}$	$69.083^{+0.022}_{-0.030}$
a ($R_\odot$)	$5.905^{+0.031}_{-0.033}$	$107.8^{+0.8}_{-0.5}$	$5.100^{+0.017}_{-0.047}$	$114.9^{+0.5}_{-1.3}$
e	$0.00211^{+0.00096}_{-0.00085}$	$0.0154^{+0.0090}_{-0.0090}$	$0.00026^{+0.00014}_{-0.00012}$	$0.289^{+0.024}_{-0.007}$
ω (deg)	129^{+22}_{-12}	$89.8^{+1.8}_{-2.5}$	69^{+57}_{-24}	$67.9^{+1.3}_{-1.0}$
i (deg)	$89.11^{+0.44}_{-0.46}$	$88.98^{+0.17}_{-0.12}$	$86.16^{+0.27}_{-0.22}$	$88.485^{+0.021}_{-0.046}$
$\mathcal{T}_0^{\rm inf/sup}$ (BJD – 2400000)	$58486.6459^{+0.0003}_{-0.0003}$	$58474.5313^{+0.0088*}_{-0.0088}$	$58492.0717^{+0.0001}_{-0.0001}$	$58512.6976^{+0.0023*}_{-0.0024}$
τ (BJD – 2400000)	$58486.231^{+0.064}_{-0.036}$	$58473.6^{+29.0}_{-31.5}$	$58491.607^{+0.116}_{-0.059}$	$58510.45^{+0.19}_{-0.13}$
Ω (deg)	0.0	$-2.81^{+3.52}_{-2.15}$	0.0	$-1.84^{+0.36}_{-0.29}$
$i_{\rm m}$ (deg)	$3.20^{+1.81}_{-2.36}$		$2.95^{+0.25}_{-0.26}$	
Mass ratio ($q = m_{\rm sec}/m_{\rm pri}$)	$0.621^{+0.005}_{-0.006}$	$0.858^{+0.011}_{-0.010}$	$0.940^{+0.003}_{-0.004}$	$0.635^{+0.004}_{-0.005}$
$K_{\rm pri}$ (km s^{-1})	$107.8^{+0.6}_{-0.7}$	$41.5^{+0.6}_{-0.3}$	$151.0^{+0.6}_{-1.4}$	$34.1^{+0.2}_{-0.2}$
$K_{\rm sec}$ (km s^{-1})	$173.8^{+1.2}_{-1.2}$	$48.3^{+0.3}_{-0.2}$	$160.6^{+0.5}_{-1.1}$	$53.8^{+0.1}_{-0.1}$
	Stellar parameters			
	Aa	Ab	B	Aa	Ab	B
	Relative quantities					
fractional radius (R/a)	$0.2744^{+0.0017}_{-0.0024}$	$0.1426^{+0.0013}_{-0.0015}$	$0.0774^{+0.0009}_{-0.0010}$	$0.2994^{+0.0014}_{-0.0011}$	$0.2642^{+0.0016}_{-0.0021}$	$0.0249^{+0.0017}_{-0.0003}$
temperature relative to $(T_{\rm eff})_{\rm Aa}$	1	$0.7593^{+0.0057}_{-0.0064}$	$0.6911^{+0.0050}_{-0.0056}$	1	$0.9819^{+0.0010}_{-0.0009}$	$0.9543^{+0.0058}_{-0.0368}$
fractional flux (in *TESS* band)	$0.1070^{+0.0008}_{-0.0008}$	$0.0122^{+0.0003}_{-0.0003}$	$0.8396^{+0.0270}_{-0.0169}$	$0.2008^{+0.0027}_{-0.0024}$	$0.1482^{+0.0014}_{-0.0019}$	$0.6340^{+0.0084}_{-0.0112}$
	Physical quantities					
m ($M_\odot$)	$1.513^{+0.025}_{-0.027}$	$0.939^{+0.012}_{-0.015}$	$2.099^{+0.066}_{-0.032}$	$1.341^{+0.012}_{-0.035}$	$1.261^{+0.013}_{-0.035}$	$1.650^{+0.028}_{-0.060}$
R ($R_\odot$)	$1.622^{+0.015}_{-0.022}$	$0.842^{+0.011}_{-0.013}$	$8.345^{+0.112}_{-0.119}$	$1.526^{+0.007}_{-0.008}$	$1.348^{+0.012}_{-0.019}$	$2.859^{+0.158}_{-0.036}$
$T_{\rm eff}$ (K)	7358^{+151}_{-87}	5590^{+61}_{-48}	5085^{+68}_{-47}	6331^{+198}_{-47}	6214^{+200}_{-43}	6028^{+52}_{-82}
$L_{\rm bol}$ ($L_\odot$)	$6.838^{+0.723}_{-0.329}$	$0.618^{+0.042}_{-0.029}$	$41.62^{+2.16}_{-1.17}$	$3.369^{+0.376}_{-0.093}$	$2.447^{+0.229}_{-0.063}$	$9.772^{+0.849}_{-0.261}$
$M_{\rm bol}$	$2.68^{+0.05}_{-0.11}$	$5.29^{+0.05}_{-0.07}$	$0.72^{+0.03}_{-0.05}$	$3.45^{+0.03}_{-0.11}$	$3.80^{+0.03}_{-0.10}$	$2.29^{+0.03}_{-0.09}$
M_V	$2.64^{+0.06}_{-0.11}$	$5.38^{+0.06}_{-0.08}$	$0.95^{+0.04}_{-0.06}$	$3.42^{+0.03}_{-0.10}$	$3.78^{+0.03}_{-0.09}$	$2.30^{+0.03}_{-0.07}$
$\log g$ (dex)	$4.199^{+0.006}_{-0.006}$	$4.559^{+0.007}_{-0.006}$	$2.919^{+0.010}_{-0.015}$	$4.196^{+0.003}_{-0.005}$	$4.278^{+0.005}_{-0.003}$	$3.744^{+0.012}_{-0.065}$
	Global system parameters					
log (age) (dex)		$9.017^{+0.022}_{-0.037}$			$9.335^{+0.014}_{-0.018}$	
[M/H] (dex)		$-0.042^{+0.048}_{-0.039}$			$0.263^{+0.085}_{-0.245}$	
$E(B-V)$ (mag)		$0.115^{+0.024}_{-0.018}$			$0.058^{+0.018}_{-0.010}$	
extra light ℓ_4 (in *TESS* band)		$0.041^{+0.017}_{-0.027}$			$0.024^{+0.019}_{-0.016}$	
$(M_V)_{\rm tot}$		$0.73^{+0.04}_{-0.07}$			$1.78^{+0.02}_{-0.08}$	
distance (pc)		2427^{+33}_{-34}			1415^{+35}_{-14}	

Note. $\mathcal{T}_0^{\rm inf/sup}$ denotes the moment of an inferior or superior conjunction of the secondary (Ab) and the tertiary (B) along their inner and outer orbits, respectively. Superior conjunctions are noted with *.

6.1.3 TIC 54060695

The outer period for this system is 60.72 d, in good agreement with the long-term mean period of 60.68 d found from the combined archival data of ASAS-SN and ATLAS. The two outer eclipses seen in the outer orbit fold of the archival data yielded an $e_{\rm out}\cos\omega_{\rm out} \simeq 0.002$, while the photodynamical fit yielded separate parameter values of $e_{\rm out} = 0.015$ and $\omega_{\rm out} = 89°$. The mutual inclination angle, $i_{\rm mut}$, between the plane of the inner EB (with period 1.0605 d) and outer orbit is $3° \pm 2°$, while the inclination angles of the individual orbital planes are both close to 89°. These are all consistent with the presence of both a primary and a secondary outer eclipse.

The tertiary star has a mass of 2.1 $M_\odot$ and is substantially evolved off the MS with a radius of 8.3 $R_\odot$. Its $T_{\rm eff}$ is only 5100 K. The two EB stars are close to 1.5 and 1 $M_\odot$, with the primary being considerably hotter at 7350 K. The giant still dominates the system's light with 85 per cent of the luminosity. These values are in decent agreement with those found from the SED fit only (see Fig. 2), but the masses are consistently lower by ∼16 per cent in the SED fit.

The photometric distance of 2427 ± 33 pc which is formally 3.4σ farther than the *Gaia* distance of 2221 ± 50 pc. The fitted value of $E(B-V)$ compares well to the one listed in Table 1. The system has an inferred age of 1.04 Gyr.

Table 5. The same as in Table 3 above, but for TIC 242132789 and TIC 456194776.

	TIC 242132789		TIC 456194776	
	Orbital elements			
	subsystem		subsystem	
	Aa–Ab	A–B	Aa–Ab	A–B
t_0 (BJD – 2400000)	58468.0		58790.0	
P (d)	$5.1287^{+0.0013}_{-0.0013}$	$42.0317^{+0.0091}_{-0.0085}$	$1.7192540^{+0.0000071}_{-0.0000075}$	$93.915^{+0.045}_{-0.038}$
a ($R_\odot$)	$16.98^{+0.13}_{-0.18}$	$81.02^{+0.68}_{-0.91}$	$8.287^{+0.019}_{-0.030}$	$143.8^{+0.4}_{-1.1}$
e	$0.01644^{+0.00041}_{-0.00042}$	$0.0055^{+0.0037}_{-0.0030}$	$0.00293^{+0.00060}_{-0.00043}$	$0.288^{+0.040}_{-0.043}$
ω (deg)	$311.4^{+2.4}_{-2.3}$	171^{+106}_{-51}	204^{+15}_{-9}	$198.9^{+2.0}_{-1.8}$
i (deg)	$88.08^{+0.47}_{-0.40}$	$89.47^{+0.14}_{-0.15}$	$89.50^{+0.39}_{-0.85}$	$88.578^{+0.035}_{-0.035}$
$\mathcal{T}_0^{\rm inf/sup}$ (BJD – 2400000)	$58470.1198^{+0.0011*}_{-0.0011}$	$58484.4801^{+0.0054}_{-0.0053}$	$58791.5538^{+0.0002}_{-0.0003}$	$58809.8646^{+0.0046*}_{-0.0046}$
τ (BJD – 2400000)	$58468.163^{+0.035}_{-0.033}$	$58471.0^{+5.0}_{-18.9}$	$58791.237^{+0.069}_{-0.041}$	$58735.9^{+1.8}_{-1.3}$
Ω (deg)	0.0	$-0.85^{+2.66}_{-0.93}$	0.0	$-1.06^{+0.71}_{-0.46}$
$i_{\rm m}$ (deg)	$2.00^{+0.88}_{-0.64}$		$1.52^{+0.40}_{-0.76}$	
Mass ratio ($q = m_{\rm sec}/m_{\rm pri}$)	$0.852^{+0.008}_{-0.008}$	$0.618^{+0.005}_{-0.005}$	$0.762^{+0.005}_{-0.005}$	$0.750^{+0.011}_{-0.020}$
$K_{\rm pri}$ (km s^{-1})	$77.0^{+0.7}_{-0.7}$	$37.3^{+0.4}_{-0.5}$	$105.4^{+0.5}_{-0.6}$	$34.5^{+0.4}_{-0.5}$
$K_{\rm sec}$ (km s^{-1})	$90.4^{+0.8}_{-1.1}$	$60.3^{+0.5}_{-0.6}$	$138.4^{+0.4}_{-0.5}$	$46.1^{+0.6}_{-0.6}$
	stellar parameters			
	Aa	Ab	B	Aa	Ab	B
	Relative quantities					
Fractional radius (R/a)	$0.1027^{+0.0018}_{-0.0018}$	$0.0712^{+0.0013}_{-0.0012}$	$0.1509^{+0.0010}_{-0.0010}$	$0.1995^{+0.0019}_{-0.0017}$	$0.1274^{+0.0013}_{-0.0013}$	$0.0344^{+0.0005}_{-0.0005}$
Temperature relative to $(T_{\rm eff})_{\rm Aa}$	1	$0.9658^{+0.0085}_{-0.0090}$	$0.7170^{+0.0102}_{-0.0074}$	1	$0.8808^{+0.0038}_{-0.0050}$	$0.8787^{+0.0065}_{-0.0082}$
Fractional flux (in *TESS* band)	$0.0597^{+0.0013}_{-0.0013}$	$0.0256^{+0.0013}_{-0.0010}$	$0.8779^{+0.0269}_{-0.0279}$	$0.1354^{+0.0028}_{-0.0028}$	$0.0368^{+0.0006}_{-0.0005}$	$0.8153^{+0.0087}_{-0.0230}$
Fractional flux (in R_C band)	–	–	–	$0.1399^{+0.0058}_{-0.0049}$	$0.0362^{+0.0012}_{-0.0014}$	$0.7944^{+0.0181}_{-0.0307}$
	Physical Quantities					
m ($M_\odot$)	$1.346^{+0.031}_{-0.045}$	$1.146^{+0.027}_{-0.034}$	$1.539^{+0.046}_{-0.060}$	$1.464^{+0.010}_{-0.015}$	$1.115^{+0.010}_{-0.014}$	$1.939^{+0.035}_{-0.056}$
R ($R_\odot$)	$1.741^{+0.031}_{-0.030}$	$1.207^{+0.029}_{-0.027}$	$12.22^{+0.12}_{-0.13}$	$1.653^{+0.017}_{-0.017}$	$1.055^{+0.012}_{-0.013}$	$4.940^{+0.066}_{-0.084}$
$T_{\rm eff}$ (K)	6568^{+101}_{-43}	6367^{+33}_{-66}	4734^{+30}_{-63}	6709^{+263}_{-138}	5924^{+176}_{-114}	5920^{+142}_{-120}
$L_{\rm bol}$ ($L_\odot$)	$5.118^{+0.266}_{-0.262}$	$2.135^{+0.154}_{-0.135}$	$67.27^{+1.79}_{-3.34}$	$5.059^{+0.708}_{-0.505}$	$1.245^{+0.131}_{-0.117}$	$27.12^{+2.54}_{-2.54}$
$M_{\rm bol}$	$3.00^{+0.06}_{-0.06}$	$3.95^{+0.07}_{-0.08}$	$0.20^{+0.06}_{-0.03}$	$3.01^{+0.11}_{-0.14}$	$4.53^{+0.11}_{-0.11}$	$1.19^{+0.11}_{-0.10}$
M_V	$2.99^{+0.06}_{-0.06}$	$3.95^{+0.07}_{-0.08}$	$0.58^{+0.10}_{-0.04}$	$2.97^{+0.11}_{-0.13}$	$4.55^{+0.12}_{-0.12}$	$1.26^{+0.10}_{-0.11}$
$\log g$ (dex)	$4.083^{+0.017}_{-0.016}$	$4.331^{+0.012}_{-0.013}$	$2.450^{+0.007}_{-0.008}$	$4.166^{+0.007}_{-0.008}$	$4.437^{+0.008}_{-0.007}$	$3.336^{+0.013}_{-0.015}$
	Global system parameters					
log (age) (dex)	$9.393^{+0.040}_{-0.053}$		$9.401^{+0.023}_{-0.023}$		$9.144^{+0.021}_{-0.019}$	
$[M/H]$ (dex)	$-0.087^{+0.072}_{-0.080}$				$0.221^{+0.089}_{-0.203}$	
$E(B-V)$ (mag)	$0.548^{+0.013}_{-0.028}$				$0.136^{+0.051}_{-0.038}$	
Extra light ℓ_4 (in *TESS* band)	$0.036^{+0.029}_{-0.026}/0.025^{+0.019}_{-0.019}$				$0.013^{+0.024}_{-0.009}$	
Extra light ℓ_4 (in R_C band)	–				$0.028^{+0.040}_{-0.019}$	
$(M_V)_{\rm tot}$	$0.42^{+0.09}_{-0.04}$				$1.01^{+0.10}_{-0.11}$	
Distance (pc)	2667^{+28}_{-28}				1609^{+23}_{-24}	

Note. $\mathcal{T}_0^{\rm inf/sup}$ denotes the moment of an inferior or superior conjunction of the secondary (Ab) and the tertiary (B) along their inner and outer orbits, respectively. Superior conjunctions are noted with *.

6.1.4 TIC 178010808

The outer orbit of TIC 178010808 has a period of 69.02 d, and is also rather flat with $i_{\rm mut} = 3^\circ \pm 0.3^\circ$, and relatively close to edge on with $i_{\rm in} = 86^\circ$, and $i_{\rm out} = 88.5^\circ$. The EB period is 0.8257 d. The eccentricity is characterized by $e_{\rm out} = 0.29$ with $\omega_{\rm out} = 68^\circ$. The outer orbit fold using the ASAS-SN, ATLAS, and WASP archival data (see Fig. 4) shows a clear detection of the primary outer eclipse, but there is merely a suggestion of a secondary outer eclipse which is not statistically significant with $e_{\rm out}\cos\omega_{\rm out} \simeq 0.16$. This is in substantial disagreement with $e_{\rm out}\cos\omega_{\rm out} \simeq 0.1$ found in the photodynamical fit.

All three stars in this system have comparable masses (within ∼20 per cent of each other). The tertiary has the largest mass at 1.65 $M_\odot$ with a slightly evolved radius of 2.9 $R_\odot$. All three stars have $T_{\rm eff} \simeq 6200K$. All the stellar parameters are in good agreement with the results of the simple SED fit which employs only minimal constraints, but the SED-fitted radius for the tertiary is about 13 per cent larger at 3.3 $R_\odot$. In either case, this is the least evolved tertiary among our set of six triples.

The photodynamic distance of 1415 ± 30 pc is in essentially perfect agreement with the *Gaia* distance (see Table 1). The fitted

Table 6. Derived ephemerides for the six triple systems to be used for planning future observations.

TIC ID	37743815	42565581	54060695	178010808	242132789	456194776
			Inner binary			
P	0.90707	1.823071	1.06049087	0.8257362	5.11458	1.719349
$\mathcal{T}_0$	8 469.101	8 469.003	8 486.635	8 492.0725	8 472.69286	8 791.552
$\mathcal{A}_{\rm ETV}$	0.001	0.002	0.001	0.001	0.011	0.007
D	0.105	0.293	0.145	0.155	0.282	0.176
			Wide binary (third-body eclipses)			
P	68.720	123.452	60.72	69.02:	41.531	93.90:
$\mathcal{T}_0^{\rm inf}$	9 224.3	8 479.1	8 504.9	8 554.2:	8 484.3	8 841.2:
$D^{\rm inf}$	1.65	3.23	2.20	0.85:	3.35	1.70:
$\mathcal{T}_0^{\rm sup}$	9 246.7:	8 543.4:	8 474.51	8 512.75	8 505.3	8 809.90
$D^{\rm sup}$	1.05:	2.30:	1.95	1.00	3.35	1.90

Note. (a) For the inner pairs: P, $\mathcal{T}_0$, $\mathcal{A}_{\rm ETV}$, D are the period, reference time of a primary minimum, half-amplitude of the ETV curve, and the full duration of an eclipse, respectively. $\mathcal{T}_0$ is given in BJD – 2 450 000, while the other quantities are in days. As all the inner eccentricities are very small and, hence, the shifts of the secondary eclipses relative to phase 0.5 are negligible (quantitatively, they are much smaller than the full durations of the individual eclipses), the same reference times and periods can be used to predict the times of the secondary eclipses. (b) For the outer orbits, we give separate reference times for the third-body eclipses around the inferior and superior conjunctions of the tertiary component. The eclipse durations, D, of the third-body eclipses do not give the extent of any specific third-body events. Rather D represents the time difference corresponding to the very first and last moments around a given third-body conjunction when the first/last contact of a third-body event may occur). Double dots (:) (1) at the outer periods of TICs 178010808 and 456194776 refer to larger uncertainties arising from the fact that in these two triples only one third-body eclipse was observed with *TESS*; (2) at superior/inferior conjunction times refer to those kinds of third-body events (i.e. primary versus secondary outer eclipses) that were not observed with *TESS*. For these events, the ephemerides are based on the archival data folds (see Fig. 4), and they might be less certain.

value of $E(B-V)$ is small at 0.058, but in agreement with the value listed in Table 1. Finally, the inferred age of the system is 2.2 Gyr.

6.1.5 TIC 242132789

The outer orbit of TIC 242132789 is the shortest among our set of six triply eclipsing triples at 41.5 d. In that sense it is the most compact of our triples and the fourth shortest period triple system known. It is also, by far the tightest of our systems with a period ratio of $P_{\rm out}/P_{\rm in}$ of only 8.2,[5] the second smallest ratio (after KIC 76668648) among all triple stellar systems where both the inner and outer periods are known with sufficient precision. TIC 242132789 is now the tightest known triple with the tertiary being the most massive component. The tertiary in the system is also the largest among our six, with R $= 12.2 \pm 0.1\,{\rm R}_\odot$. This implies that $R_B/a \simeq 0.15$ so perhaps it is not surprising that the outer orbit has nearly circularized with $e_{\rm out} = 0.006$. The mutual inclination angle is marginally significantly different from zero at $i_{\rm mut} = 2.0^{+0.9}_{-0.6}$ degrees. The two orbital inclination angles are $i_{\rm in} = 88.1^\circ$ and $i_{\rm out} = 89.5^\circ$.

All three stellar components were originally F stars with the tertiary just higher enough in mass (1.54 $\rm M_\odot$) to have evolved well off the main sequence while the EB primary, at 1.35 $\rm M_\odot$ is only slightly evolved. The SED fit is in agreement with these basic facts, but it yields $R_B = 15.6 \pm 1.6\,{\rm R}_\odot$, just barely consistent with the photodynamical analysis, and the primary EB mass is lower by 25 per cent compared to the photodynamical results. Much of this discrepancy may be attributed to the fact that the SED fit yields a distance of 3250 pc, which in excellent agree with *Gaia*, while the photodynamical solution prefers a much closer distance.

[5]We define the 'tightness' of a binary as $P_{\rm out}/P_{\rm in}$, where the smaller the ratio, the tighter the binary. In this case, as a technical matter, we use the ratio of periods from Table 5.

In fact, the photodynamic distance is 2667 ± 28 pc. This is to be compared to the *Gaia* distance of 3258 ± 165 pc. This is formally a 3.6σ discrepancy, and may partially be accounted for if the *Gaia* measurement is affected by the EB stars that contribute 10 per cent of the system light. The fitted $E(B-V)$ is close to 0.55, while the value from Table 1 is lower at 0.34. The age of the system is found to be 2.5 Gyr.

This system exhibits the largest ETVs among our sample of triples. The amplitude is 0.01 d with a period of $P_{\rm out}/2 \simeq 21$ d. The ETV curve for this source is explored further in Appendix A.

6.1.6 TIC 456194776

This system has an outer orbital period of 93.83 d found from the ASAS-SN and ATLAS archival data, which, in turn, is in excellent agreement with the period found from the photodynamical modelling (93.90 d). The EB period is 1.7193 d. The mutual inclination angle between the inner binary and the outer orbit is 1.5°, while $i_{\rm in}$ and $i_{\rm out}$ are 89.5° and 88.6°, respectively. Again, this is a flat and edge on system. The parameter $e\cos\omega_{\rm out}$ based on the fold of the outer orbit using ASAS-SN and ATLAS data is 0.26. By comparison the individual components from the photodynamical fits are: $e = 0.29$ and $\omega_{\rm out} = 199^\circ$, leading to $|e\cos\omega_{\rm out}| = 0.27$, which is in excellent agreement.

The mass of the tertiary is 1.9 $\rm M_\odot$ and its evolved radius is 4.9 $\rm R_\odot$. The EB stars are near the main sequence with lower masses of 1.5 and 1.1 $\rm R_\odot$. The EB primary is considerably hotter at 6700 K than the evolved tertiary at 5900 K. The SED fit alone yields somewhat hotter EB stars with 16 per cent higher mass, and good agreement with the photodynamical fit for the radius of the tertiary.

The photometric distance of 1609 pc is in excellent agreement with the *Gaia* value of 1590 pc, given that both uncertainties are of order 30 pc. The fitted photodynamical and MAST values for $E(B-V)$

of 0.14 versus 0.17, respectively, are in quite reasonable agreement. The system age is 1.4 Gyr.

This was the one triple system in this work for which we also obtained radial velocity data. We explore in Appendix A2 how the RVs added to the photodynamical solution.

6.2 Common Properties

What all of these six triply eclipsing triple systems have in common is that they are all remarkably flat with $i_{\rm mut}$ within a couple of degrees of zero. In fact, only one of these systems has $i_{\rm mut} \gtrsim 3^\circ$ and that is TIC 42565581 where $i_{\rm mut} = 5.5^\circ \pm 1.6^\circ$. The inclination angles of the EB plane and the outer orbit are all within a few degrees of 90°, and, of course, that is a strong selection effect since we are searching for outer eclipses as a definitive signature of this type of system.

The orbital periods of the six systems are, in order, 41.5, 60.7, 68.7, 69.0, 93.9, and 123.5 d. As a measure of how compact these systems are, we note that there are only 8 other triple systems known with comparably short periods (see e.g. Borkovits et al. 2022). By contrast, only one of our systems is considered 'tight', i.e. with a small value of $P_{\rm out}/P_{\rm in}$. Specifically, five of the six systems have $P_{\rm out}/P_{\rm in}$ in the range of 55–83, while TIC 242132789 is unique in this group with a quite small value of $P_{\rm out}/P_{\rm in} = 8.2$. This is the second tightest triple known.

Two of the outer orbits of the six triples have notably small eccentricities ($e \lesssim 0.02$). It is interesting that in these two cases, the value of $R_B/a_{\rm out}$ is 0.077 for TIC 54060695 and 0.151 for TIC 242132789. Therefore, it seems likely that tidal circularization may have played a role in the circularization of these systems where the tertiary is both large and substantially convective. For the other four systems, $R_B/a_{\rm out}$ ranges from 0.025 to 0.040.

The tertiary masses in these systems range from 1.6 to 2.2 $M_\odot$, and are all evolved off the main sequence. They have radii between 2.9 and 12 $R_\odot$. Their evolutionary ages all range from 1.0–2.5 Gyr. The large radii of the tertiary stars are also something of a selection effect. The probability of outer eclipses in these systems is roughly proportional to $R_B/a_{\rm out}$. Thus, for similar orbital separations as in these systems (50–100 $R_\odot$), the outer eclipse probability can be enhanced by nearly an order of magnitude for the size of the tertiaries we have found as compared to when they were on the main sequence.

7 SUMMARY AND DISCUSSION

In this paper, we report the discovery and analyses of six triply eclipsing triple systems found from observations with the *TESS* space telescope. They were observed during one to three *TESS* sectors each, yielding precise space-borne photometric data trains. In four cases, the source was observed during two sectors, but those sectors were separated by two years. However, when combined with archival ground-based survey photometric measurements (see Fig. 4), we were able to obtain reasonably accurate orbital and stellar parameters for all six triple systems via detailed photodynamical analyses.

This is part of an ongoing programme to find and characterize compact triple systems via their signature third-body eclipses. In all we have found 52 such systems during the first three *TESS* cycles. For 20 of these there is sufficient archival data (typically from ASAS-SN and ATLAS, but also including WASP, KELT, and MASCARA) to have determined unambiguously the outer orbit via the long-term detection of third-body eclipses. Generally, with *TESS* we see only one or two third-body events because of the sparse coverage, and even when there are two such events, they are sufficiently far apart (i.e. two years), that the outer period is at best ambiguous. There is of course, the additional possibility that even if two eclipses are seen with *TESS*, they are not of the same type, i.e. primary versus secondary. Of the 20 triply eclipsing triples where we now know the outer period, we have chosen six more of them from this extensive set to report here.[6] This choice of six sources was to strike a balance between being able to discuss each one in some detail, without making the paper too lengthy.

The vast majority of the triply eclipsing systems that we have discovered in the *TESS* data have been found via visual surveys of the light curves by the VSG group (Kristiansen et al. 2022). We employ both a machine learning (ML) approach (Powell et al. 2021) and a direct visual search in looking for multistellar systems. Empirically, we have found that the ML approach is superior for finding large numbers of EBs within the millions of *TESS* light curves, but that the visual approach is substantially more efficient at finding non-repeating, and odd shaped third-body eclipses. In all, the VSG has surveyed some 10 million light curves, while finding 52 with a triply eclipsing triples signature as well as many other interesting and unique phenomena (see Kristiansen et al. 2022). We anticipate that our list of triply eclipsing triples will grow roughly linearly with time as more of the *TESS* light curves are inspected.

Most of the definitive determinations of the outer orbital periods were made using BLS transforms of archival ground-based photometric data sets, after the existence of third-body events was established from the *TESS* data. This raises the question of whether there is a way to find the third-body eclipses directly in these archival data sets without first knowing that they are present in a particular source. We are fairly certain that most triple star systems exhibiting eclipses of the tertiary will also contain an eclipsing binary. In that case the dominant source of 'noise' in a BLS is from the presence of the much higher duty cycle orbital modulations. In order to detect the third-body events in the archival data, it is generally necessary to first subtract out the EB light curve. While it is possible to automate such a search and removal operation, it seems more efficient at this point to spot the existence of the third-body events first in the precision photometry of the *TESS* data set.

Now that these triply eclipsing triples are known, and their basic parameters determined, more focused follow-up ground-based photometry, especially with small amateur telescopes, would be welcome. All six objects have G magnitudes in the range of 12.2–13.5. The ordinary primary eclipse depths range from 2 to 15 per cent, while the third-body eclipses range from a few to 25 per cent deep. The ETV data from *TESS* itself was typically instrumental in determining some of the parameters found from the photodynamical analyses. Thus, future timing observations of the ordinary EB eclipses in these systems would be quite helpful in improving the parameter determinations. The dynamical delays in these systems range from 0.1 to 14 min, while the LTTE delays are typically ∼2 min, so readily within the realm of amateur observations. Searches for additional third-body events are difficult without advance approximate predictions since they occur relatively infrequently. In order to facilitate ground-based follow up observations of future third-body events, we provide ephemerides for such observations in Table 6. In some cases, however, these ephemerides are somewhat uncertain, and therefore, we recommend dedicated observations within a wider time domain around each forecasted mid-third-body-eclipse time. Because of the flatness of all these systems, we predict that there will

[6]Four of the sources from this collection have been reported previously in Borkovits et al. (2020a, 2022).

Table 7. Evolution times in Myr of the tertiary stars.

Phase	1.5 $M_\odot$	2.0 $M_\odot$	2.5 $M_\odot$
3.0 $R_\odot$ → tip of RGB	247	61	13
8.0 $R_\odot$ → tip of RGB	86	37	8
15 $R_\odot$ → tip of RGB	28	26	4
Giant → AGB	126	300	200
Total evolution	2900	1350	780

Note. All times were computed with the MESA stellar evolution code. 2.5 $M_\odot$ stars will not attain sufficiently large radii to fill their Roche lobes during the ascent of the RGB in the systems under discussion.

be no eclipse-depth variations either to search for or to cause long 'outages' of eclipses.

The six systems discussed in this work are relatively old, of the order of 1 to a few Gyr. They are manifestly dynamically stable and will last until the tertiary overflows its Roche lobe. In principle, the EB stars could also evolve to mass exchange, but the tertiaries in these systems are sufficiently more massive, and already evolved so that they will fill their Roche lobes, which range in size from 36 to 51 $R_\odot$, before the EB stars grow by even 10 per cent in size. Generally, once a star of ∼1.5–2.5 $M_\odot$ has grown to 3–12 times its original radius, we can expect it to fully ascend the giant branch within a small fraction of its total lifetime. These lifetimes are illustrated in Table 7. They also illustrate the fraction of time that systems like these have tertiary stars that are substantially evolved, and hence easier in which to detect third-body eclipses. For example, a 2 $M_\odot$ tertiary that has $R \gtrsim 8\,R_\odot$ spends only 37/1350 = 2.7 per cent of its total lifetime in this state.

As mentioned above the VSG group (Kristiansen et al. 2022) has visually examined the light curves of some 9 million anonymous *TESS* light curves as well as 1 million *TESS* light curves of preselected EBs (see Powell et al. 2021; Kruse et al., in preparation). In all, they have found 52 triply eclipsing triples with periods in the range of ∼42–300 d. Thirty-two of these were found among the EB light curves, and only 20 from among the much more numerous anonymous light curves. If each target was observed, on average, during two *TESS* sectors spanning about 50 d, then the probability of finding a third-body event in at least one of those sectors is of order 50 per cent, especially when we consider that a fair fraction of the systems exhibit both types of outer eclipses (i.e. primary and secondary). Here, we focus on the 32 systems found from among the pre-selected EB light curves. This suggests a 'success rate' of 3×10^{-5} per EB. In order to assess, the actual fraction of EBs that contain a third body in a compact outer orbit that is coaligned with the inner binary, we use a simple Monte Carlo approach. This takes into account: (i) the probability of being at the right outer orbital phase to see a third-body eclipse in 50 d of observing; (ii) the fraction of triply eclipsing systems missed because even if the three stars are in a perfectly flat configuration it is possible to detect only EB eclipses; and (iii) the detection enhancement because some of the tertiary stars are evolved, i.e. larger than their MS radius. We find that a fraction equal to 2×10^{-4} of all close binaries (period = 0.5–20 d) host a third star in a compact 2 + 1 triple configuration that is flat. Thus, while these are relatively fairly rare systems, there are probably several hundred thousand of them in the Galaxy.

Again, as we have suggested throughout the paper, selection effects favour (i) compact systems, (ii) at least partly flat architecture, and (iii) somewhat evolved tertiaries to enhance the outer eclipse probability. Thus, it is not surprising that these are the systems we have predominantly spotted while surveying the light curves.

We have found that the masses of all the stars in the triples we studied are the same to within small factors of order 2. Otherwise, the EB might not have been detected in the glare of a much more luminous tertiary. Comparable masses and short outer periods imply an accretion-driven migration formation scenario (see e.g. Tokovinin 2021 and references therein). In the latter case, the flatness of the systems might demonstrate that such migration is accompanied by orbit alignment. Comparable masses also imply accretion from a common gas source. This mechanism predicts that the outer mass ratio must not exceed unity, and this is indeed the case for the systems presented here. Moderate outer eccentricities as we observe in 4 of the 6 systems can be largely primordial, although circularization by tides in giants also works in some cases (e.g. for TIC 54060695 and TIC 242132789 as we mentioned earlier).

There is also a possible link between our triple systems and 2 + 2 compact quadruples. Some giants in these triple systems could have originally been second binaries that have merged. This can be revealed by apparent difference of ages, as hinted at in one of our systems: TIC 42565581, though the evidence there is only marginal. These six triples with giant tertiaries, favored by observational selection, are also favourable candidates for a triple common envelope phase in the future. In this latter regard, see the studies by Toonen & Nelemans (2013) and Hamers et al. (2022), with emphasis on triple common envelope evolution (Glanz & Perets 2021) and its end products.

Finally, we note that in terms of stellar evolution theory, the tertiary in these systems fixes their age. Thus, we obtain a triplet of reasonably accurate masses and radii with a known age.

ACKNOWLEDGEMENTS

We are grateful to Andrei Tokovinin for going through the manuscript and making some very helpful suggestions for how to interpret our findings.

We thank Allan R. Schmitt and Troy Winarski for making their light curve examining software tools LcTools and AKO-TPF freely available.

VBK is thankful for support from NASA grants 80NSSC21K0351.

TB and ZG acknowledge the support of the Hungarian National Research, Development and Innovation Office (NKFIH) grant K-125015, a PRODEX Experiment Agreement No. 4000137122 between the ELTE Eötvös Loránd University and the European Space Agency (ESA-D/SCI-LE-2021-0025), and the support of the city of Szombathely. ZG acknowledges the Lendület LP2018-7/2021 grant of the Hungarian Academy of Science, the VEGA grant of the Slovak Academy of Sciences No. 2/0031/22, the Slovak Research and Development Agency contract No. APVV-20-0148.

AP acknowledges the financial support of the Hungarian National Research, Development and Innovation Office – NKFIH Grant K-138962.

We thank David Latham for facilitating the TRES observations of TIC 456194776.

The operation of the BRC80 robotic telescope of Baja Astronomical Observatory has been supported by the project 'Transient Astrophysical Objects' GINOP 2.3.2-15-2016-00033 of the National Research, Development and Innovation Office (NKFIH), Hungary, funded by the European Union.

This paper includes data collected by the *TESS* mission. Funding for the *TESS* mission is provided by the NASA Science Mission directorate. Some of the data presented in this paper were obtained from the Mikulski Archive for Space Telescopes (MAST). STScI is operated by the Association of Universities for Research in

Astronomy, Inc., under NASA contract NAS5-26555. Support for MAST for non-*HST* data is provided by the NASA Office of Space Science via grant NNX09AF08G and by other grants and contracts.

We have made extensive use of the All-Sky Automated Survey for Supernovae archival photometric data. See Shappee et al. (2014) and Kochanek et al. (2017) for details of the ASAS-SN survey.

We also acknowledge use of the photometric archival data from the Asteroid Terrestrial-impact Last Alert System (ATLAS) project. See Tonry et al. (2018) and Heinze et al. (2018) for specifics of the ATLAS survey.

This work has made use of data from the European Space Agency (ESA) mission *Gaia*,[7] processed by the *Gaia* Data Processing and Analysis Consortium (DPAC).[8] Funding for the DPAC has been provided by national institutions, in particular the institutions participating in the *Gaia* Multilateral Agreement.

This publication makes use of data products from the *Wide-field Infrared Survey Explorer*, which is a joint project of the University of California, Los Angeles, and the Jet Propulsion Laboratory/California Institute of Technology, funded by the National Aeronautics and Space Administration.

This work also makes use of data products from the Two Micron All Sky Survey, which is a joint project of the University of Massachusetts and the Infrared Processing and Analysis Center/California Institute of Technology, funded by the National Aeronautics and Space Administration and the National Science Foundation.

We used the Simbad service operated by the Centre des Données Stellaires (Strasbourg, France) and the ESO Science Archive Facility services (data obtained under request number 396301).

DATA AVAILABILITY

The *TESS* data underlying this article were accessed from MAST (Barbara A. Mikulski Archive for Space Telescopes) Portal (https://mast.stsci.edu/portal/Mashup/Clients/Mast/Portal.html). The ASAS-SN archival photometric data were accessed from https://asas-sn.osu.edu/. The ATLAS archival photometric data were accessed from https://fallingstar-data.com/forcedphot/queue/. A part of the data were derived from sources in the public domain as given in the respective footnotes. The derived data generated in this research and the code used for the photodynamical analysis will be shared upon a reasonable request to the corresponding author.

REFERENCES

Alonso R., Deeg H. J., Hoyer S., Lodieu N., Palle E., Sanchis-Ojeda R., 2015, A&A, 584, L8
Bailer-Jones C. A. L., Rybizki J., Fouesneau M., Demleitner M., Andrae R., 2021, AJ, 161, 147
Bakos G. Á., Lázár J., Papp I., Sári P., Green E. M., 2002, PASP, 114, 974
Bianchi L., Shiao B., Thilker D., 2017, ApJS, 230, 24
Borkovits T., Érdi B., Forgács-Dajka E., Kovács T., 2003, A&A, 398, 1091
Borkovits T. et al., 2013, MNRAS, 428, 1656
Borkovits T., Rappaport S., Hajdu T., Sztakovics J., 2015, MNRAS, 448, 946
Borkovits T., Hajdu T., Sztakovics J., Rappaport S., Levine A., Bíró I. B., Klagyivik P., 2016, MNRAS, 455, 4136
Borkovits T. et al., 2018, MNRAS, 478, 5135
Borkovits T. et al., 2019a, MNRAS, 483, 1934
Borkovits T., Sperauskas J., Tokovinin A., Latham D. W., Csányi I., Hajdu T., Molnár L., 2019b, MNRAS, 487, 4631
Borkovits T. et al., 2021, MNRAS, 503, 3759
Borkovits T., 2022, Galaxies, 10, 9
Borkovits T. et al., 2020a, MNRAS, 493, 5005
Borkovits T. et al., 2020b, MNRAS, 496, 4624
Borkovits T. et al., 2022, MNRAS, 510, 135
Borucki W. J. et al., 2010, Science, 327, 977
Bouma L., Hartman J., Bhatti W., 2019, ApJS, 245, 13
Bressan A. et al., 2012, MNRAS, 427, 127
Buchhave L. A. et al., 2010, ApJ, 720, 1118
Carter J. A. et al., 2011, Science, 331, 562
Castelli F., Kurucz R. L., 2003, in Piskunov N., Weiss W.W., Gray D. F., eds, Proc. IAU Symp. 210, Modelling of Stellar Atmospheres. Astron. Soc. Pac., San Francisco, p. A20
Chambers K. C. et al., 2016, preprint (arXiv:1612.05560)
Choi J., Dotter A., Conroy C., Cantiello M., Paxton B., Johnson B. D., 2016, ApJ, 823, 102
Cutri R. M. et al., 2013 wise.rept, 1C
Dotter A., 2016, ApJS, 222, 8
Fausnaugh M. M., Burke C. J., Ricker G. R., Vanderspek R., 2020, Research Notes of the AAS, 4, 251
Ford E. B., 2005, AJ, 129, 1706
Furesz G., 2008, PhD thesis, Univ. Szeged
Gaia Collaboration et al., 2021, A&A, 649, A1
Glanz H., Perets H. B., 2021, MNRAS, 500, 1921
Green G. M., Schlafly E. F., Zucker C., Speagle J. S., Finkbeiner D. P., 2019, ApJ, 887, 93
Gunn J. E. et al., 1998, AJ, 116, 3040
Hammers A. S., Perets H. B., Thompson T. A., Neunteufel P., 2022, ApJ, 925, 178
Heinze A. N. et al., 2018, AJ, 156, 241
Henden A. A., Levine S., Terrell D., Welch D., 2015, American Astronomical Society, AAS Meeting #225, id.336.16
Howell S. B. et al., 2014, PASP, 126, 398
Huang C. X. et al., 2020, RNAAS, 4, 206
Jenkins J. M. et al., 2016, Software and Cyberinfrastructure for Astronomy IV, Volume 9913. International Society for Optics and Photonics. SPIE, Bellingham, p. 99133E
Klinglesmith D. A., Sobieski S., 1970, AJ, 75, 175
Kochanek C. S. et al., 2017, PASP, 129, 104502
Kostov V. B. et al., 2021, ApJ, 917, 93
Kostov V. B. et al., 2022, ApJS, 259, 66
Kovács G., Zucker S., Mazeh T., 2002, A&A, 391, 369
Kozai Y., 1962, AJ, 67, 591
Kristiansen M. H. et al., 2022, PASP
Latham D. W. et al., 2002, AJ, 124, 1144
Lidov M. L., 1962, Planetary Space Sci., 9, 719
Lucy L. B., 1967, Zeitschrift für Astrophys., 65, 89
Masuda K., Uehara S., Kawahara H., 2015, ApJ, 806, L37
Mitnyan T., Borkovits T., Rappaport S., Pál A., Maxted P. F. L., 2020, MNRAS, 498, 6034
Nardiello D. et al., 2019, NNRAS, 490, 3806
Nordström B. et al., 1994, A&A, 287, 338
Ochsenbein F., Bauer P., Marcout J., 2000, A&AS, 143, 23
Oelkers R. J., Stassun K. G., 2018, AJ, 156, 132
Orosz J., 2015, ASPC, 496, 55
Paegert M. et al., 2021, preprint (arXiv:2108.04778)
Pál A., 2012, MNRAS, 421, 1825
Paxton B., Bildsten L., Dotter A., Herwig F., Lesaffre P., Timmes F., 2011, ApJS, 192, 3
Paxton B. et al., 2015, ApJS, 220, 15
Paxton B. et al., 2019, ApJS, 243, 10
Pepper J. et al., 2007, PASP, 119, 923
Pepper J. et al., 2012, PASP, 124, 230
Pollacco D. L. et al., 2006, PASP, 118, 1407
Powell B. P. et al., 2021, AJ, 161, 162
Prša A., Zwitter T., 2005, ApJ, 628, 426

[7] https://www.cosmos.esa.int/gaia
[8] https://www.cosmos.esa.int/web/gaia/dpac/consortium

Rappaport S. et al., 2021, MNRAS, 503, 254
Ricker G. R. et al., 2015, JATIS, 1, 014003
Rowden P. et al., 2020, AJ, 160, 76
Schmitt A. R., Hartman J. D., Kipping D. M., 2019, preprint (arXiv:1910.08034)
Shappee B. J. et al., 2014, ApJ, 788, 48
Skrutskie M. F. et al., 2006, AJ, 131, 1163
Smith K. W. et al., 2020, PASP, 132, 5002
Talens G. J. J., Spronck J. F. P., Lesage A.-L., Otten G. P. P. L., Stuik R., Pollacco D., Snellen I. A. G., 2017, A&A, 601, A11
Tokovinin A., 2021, Universe, 7, 352
Tonry J. L. et al., 2018, PASP, 130, 4505
Toonen S., Nelemans G., 2013, A&A, 557, 87
von Zeipel H., 1910, AN, 183, 345
Wolf C. et al., 2018, PASA, 35, 10

SUPPORTING INFORMATION

Supplementary data are available at *MNRAS* online.

suppl_data

Please note: Oxford University Press is not responsible for the content or functionality of any supporting materials supplied by the authors. Any queries (other than missing material) should be directed to the corresponding author for the article.

APPENDIX A: SUPPLEMENTARY MATERIAL – RV AND ETV FITS

A1 Interpretation of the large amplitude ETV of TIC 242132789

As was mentioned in Section 5, the analysis of the ETV curves that are extracted from the high-precision *TESS* light curves are inherent in our photodynamical analyses. They provide very strict constraints on the eclipsing periods of the inner EBs and, in the case of some eccentricities, the parameters $e_{\rm in}\cos\omega_{\rm in}$ are also very strictly constrained through these data. In the case of five of the six investigated systems, however, due to the very short durations of the *TESS* observations, the ETV curves do not carry any useful information about the outer orbits nor, therefore, on the system configurations. The only exception is the ETV curve of TIC 242132789 that exhibits large amplitude ($\mathcal{A}_{\rm ETV} \sim 0\overset{\rm d}{.}01$), quasi-sinusoidal variations with a period that is exactly half of the outer orbital period, $P_{\rm out}$ (see Fig. A1). Here, we briefly discuss the origin of this timing variation, and its implications for the analytic perturbation theories of hierarchical triple systems.

First, it is evident that this ETV cannot arise from the well-known geometric light-traveltime effect (LTTE), for at least three reasons. (1) The LTTE has the same period as the outer period. (2) Since in this system the outer orbit is found to be almost circular, the third-body eclipses should have occurred at the extrema of an LTTE generated ETV curve, while, as is seen in Fig. A1, the *TESS*-observed third-body events occurred approximately mid-way between the two extrema. Finally (3), with the use of the masses and orbital elements found from the photodynamical analysis (Table 5) one can calculate the expected amplitude of the LTTE as being $\mathcal{A}_{\rm LTTE} \sim 10^{-3}$ d, i.e. one order of magnitude smaller than is observed.

Secondly, it is also clear that the ETV cannot be the consequence of the usually considered medium-period class perturbations of the tertiary.[9] It was shown by Borkovits et al. (2003) that in a coplanar, doubly circular hierarchical triple system (like TIC 242132789) the largest amplitude, quadruple-order perturbations disappear. This finding was confirmed later with the analyses of the recently discovered, doubly circular, coplanar, triply eclipsing triple systems such as HD 181068 (Borkovits et al. 2013), TIC 278825952 (Mitnyan et al. 2020), and TIC 193993801 (Borkovits et al. 2022). Moreover, though it was found by Borkovits et al. (2015) that the octuple-order perturbation terms do not vanish for such a scenario, their characteristic periods are $P_{\rm out}$ and/or $P_{\rm out}/3$, but not the half of the orbital period.

On the other hand, as was also discussed in Borkovits et al. (2015), for the tightest triple systems the strict hierarchical approximation no longer remains fully valid. This fact makes it necessary to include some further terms that are denoted as '$P_{\rm out}$ time-scale residuals of the $P_{\rm in}$ time-scale dynamical effects'. According to their calculations (equations 20 and 21), the leading term of this expression for a doubly circular, coplanar configuration gives the following ETV

[9] In hierarchical triple systems, the periodic perturbations have three different classes, according to their characteristic time-scales, as (i) short period ones with characteristic time-scale of $P_{\rm in}$, (ii) medium period ones, having time-scale of $P_{\rm out}$, and (iii) long period perturbations, which are effective on a time-scale of $P_{\rm out}^2/P_{\rm in}$.

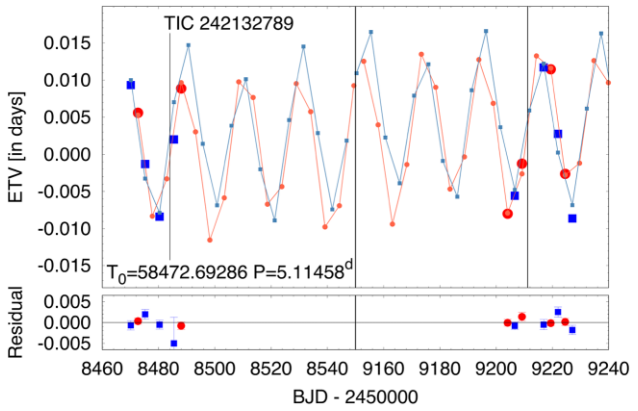

Figure A1. Photodynamical fit to the *TESS* ETV curves for TIC 242132789. Note the high amplitude of the ETVs and the fact that they oscillate at twice the frequency of the outer orbit (i.e. every ∼21 d). The larger and darker red circles and blue squares represent the observed primary and secondary times of EB eclipses, while the smaller, lighter symbols, connected with straight lines, are taken from the photodynamical model ETV curve. The two thin vertical lines denote the locations of the two third-body outer eclipses. Residuals are also shown in the lower panel, where the uncertainty on each point is also noted.

Table A1. Measured radial velocities of the tertiary component of TIC 456194776. The date is given as BJD – 2 450 000, while the RVs and their uncertainties are in km s^{-1}.

Date	RV_B	σ_B	Date	RV_B	σ_B
9478.950099	– 57.49	1.70	9527.793497	29.48	4.65
9488.905299	– 49.90	3.77	9531.733497	20.00	1.69
9493.853498	– 26.85	2.08	9534.827997	25.57	3.51
9497.825098	– 12.50	2.92	9546.797096	12.98	2.88
9504.781298	17.93	2.34	9557.734596	– 2.03	2.48
9507.755898	15.05	1.62	9567.663896	– 36.08	2.18
9514.843597	31.94	3.20	9582.678395	– 52.31	2.10
9519.872897	26.39	2.15	9591.693095	– 22.35	1.94
9521.876697	32.75	2.31	9596.620294	– 1.33	2.62
9524.771097	23.14	2.26	9605.728294	15.71	1.51

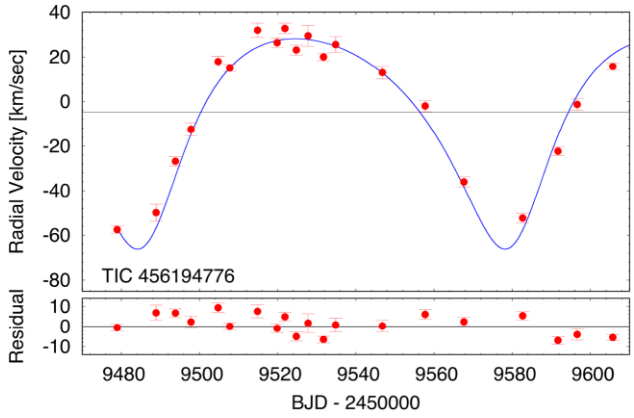

Figure A2. Photodynamical fit to the 20 TRES radial velocity data points for TIC 456194776. The RVs points with uncertainties are given in Table A1. The blue curve is from the spectro-photodynamical analysis described in Section 5.

contribution:

$$\Delta_{\rm short} = \frac{11}{16\pi}\frac{m_{\rm B}}{m_{\rm AB}}\frac{P_{\rm in}^3}{P_{\rm out}^2}\sin\left[2\frac{2\pi}{P_{\rm out}}\left(t-\mathcal{T}_{\rm out}^{\rm inf}\right)\right]. \quad \text{(A1)}$$

Substituting the third-body ($m_{\rm B}$) and the total system ($m_{\rm AB}$) masses, as well as the inner and outer periods ($P_{\rm in,\,out}$) from Table 5, one readily finds for the amplitude that $\mathcal{A}_{\rm short} = 0\overset{\rm d}{.}0064$, which is close to the observed value. Moreover, the expression above describes well not only the amplitude and period of the observed ETV, but also its phase. And, according to equation (A1), both kinds of third-body eclipses should occur mid-way between the lower and upper extrema of the ETV curve, as is very nicely demonstrated in Fig. A1. Therefore, we may conclude that the large amplitude ETV in the case of TIC 242132789 originates from this latter effect. On the other hand, the fact that the theoretically computed amplitude is only about two-thirds of the observed value, may serve as a cautionary note. And, some further more sophisticated theoretical modelling may be worthwhile for the correct analytical description of the ∼ month-timescale perturbations of the tightest triple star systems.

A2 A more in-depth analysis of TIC 456194776, including ground based RV data

Late in the production of this paper, we were fortunate enough to acquire a significant number of radial velocity measurements of this target. We obtained spectroscopic observations of the target TIC 456194776 with the Tillinghast Reflector Echelle Spectrograph (TRES; Furesz 2008), on the 1.5-m reflector at the Fred Lawrence Whipple Observatory (FLWO) in Arizona USA. TRES is a high-resolution fiber-fed echelle spectrograph, with a spectral resolving power of $R = 44000$ over the wavelength region of 3900–9100 Å. A total of 20 observations were obtained of TIC 456194776 between 2021 September 21 and 2022 January 26, with signal-to-noise ratios per resolution element of 23–40 in the Mgb triplet wavelength region (∼5187 Å). The spectra were extracted and reduced as per Buchhave et al. (2010), with wavelength solutions derived from bracketing Th-Ar lamp exposures. Visual inspection of the spectra revealed only the lines of the brighter tertiary (star B). Radial velocities were derived by cross-correlation against a suitable synthetic template from a large pre-computed library based on model atmospheres by R. L. Kurucz, and a line list tuned to better match real stars (see Nordström et al. 1994; Latham et al. 2002). These templates cover a limited wavelength region near the Mg b triplet. We find the tertiary to be a rapidly rotating star with an estimated $v \sin i$ of about 80 km s^{-1}.

The 20 radial velocities and their uncertainties are given in Table A1, while the RV points are plotted in Fig. A2. The solid blue curve is the photodynamical fit that was produced during the analysis that led up to the MDR (model-dependent-with-RVs) solution discussed in Section 5.

In Table A2, we compare the photodynamical fits for TIC 4561944776 using both the MDN and MDR models. Recall that in the latter we add the RV points to the analysis in addition to the

Table A2. TIC 456194776: abbreviated parameter comparison between MDR and MDN models.

	MDR			MDN		
			Orbital elements			
	Subsystem			Subsystem		
	Aa–Ab		A–B	Aa–Ab		A–B
a ($R_\odot$)	$8.282^{+0.021}_{-0.029}$		$143.5^{+0.49}_{-0.32}$	$8.287^{+0.019}_{-0.030}$		$143.8^{+0.4}_{-1.1}$
e	$0.00437^{+0.00058}_{-0.00057}$		$0.314^{+0.011}_{-0.010}$	$0.00293^{+0.00060}_{-0.00043}$		$0.288^{+0.040}_{-0.043}$
ω (deg)	$231.3^{+4.9}_{-5.6}$		$197.2^{+1.3}_{-1.5}$	204^{+15}_{-9}		$198.9^{+2.0}_{-1.8}$
i (deg)	$88.36^{+0.28}_{-0.63}$		$88.544^{+0.038}_{-0.042}$	$89.50^{+0.39}_{-0.85}$		$88.578^{+0.035}_{-0.035}$
Ω (deg)	0.0		$0.24^{+0.50}_{-0.41}$	0.0		$-1.06^{+0.71}_{-0.46}$
γ (km s^{-1})	$-4.93^{+0.21}_{-0.20}$			–		
			Stellar parameters			
	Aa	Ab	B	Aa	Ab	B
			Physical quantities			
m ($M_\odot$)	$1.468^{+0.011}_{-0.013}$	$1.106^{+0.011}_{-0.014}$	$1.913^{+0.026}_{-0.028}$	$1.464^{+0.010}_{-0.015}$	$1.115^{+0.010}_{-0.014}$	$1.939^{+0.035}_{-0.056}$
R ($R_\odot$)	$1.666^{+0.017}_{-0.022}$	$1.047^{+0.018}_{-0.014}$	$4.947^{+0.085}_{-0.072}$	$1.653^{+0.017}_{-0.017}$	$1.055^{+0.012}_{-0.013}$	$4.940^{+0.066}_{-0.084}$
$T_{\rm eff}$ (K)	6870^{+191}_{-123}	6004^{+158}_{-93}	5944^{+168}_{-72}	6709^{+263}_{-138}	5924^{+176}_{-114}	5920^{+142}_{-120}
			Global system parameters			
log (age) (dex)		$9.141^{+0.007}_{-0.015}$			$9.144^{+0.021}_{-0.019}$	
distance (pc)		1609^{+33}_{-25}			1609^{+23}_{-24}	

Table B1. Eclipse Times of TIC 37743815.

BJD −2 400 000	Cycle no.	std. dev. (*d*)	BJD −2 400 000	Cycle no.	Std. dev. (*d*)	BJD −2 400 000	Cycle no.	Std. dev. (*d*)
58469.100180	0.0	0.017417	58485.427452	18.0	0.000927	59211.083151	818.0	0.000716
58470.005584	1.0	0.000922	58486.334080	19.0	0.001151	59211.992122	819.0	0.001195
58470.912387	2.0	0.001245	58487.244723	20.0	0.000905	59212.899021	820.0	0.001022
58471.820704	3.0	0.001031	58488.148083	21.0	0.001237	59213.807149	821.0	0.000824
...	...	...	...	...	...	...	...	...

photometry, ETV points, SED data, and the use of stellar evolution tracks and model atmospheres. Of all the parameters that we compute, we limit the ones that are compared in the table to only five orbital, three stellar, and two global system parameters, as illustrative and representative. This comparison serves as a direct 'calibration' as to how well we can do without the RVs. All of the stellar and global parameters agree to within 1 mutual σ of the two solutions. Likewise, among the orbital elements, the a, i, and Ω values agree to within just somewhat more than 1σ. The two most interesting differences are in $\omega_{\rm in}$ and the eccentricities. In particular the two models differ in $e_{\rm in}$ by 1.7 σ. For $e_{\rm out}$, where the RV data points help most directly, the two model values differ by only $1/2\sigma$. We see that the two values of $\omega_{\rm in}$ differ by 1.7σ. Thus, overall, we find the models with and without the use of RVs to be in quite substantial agreement. Finally, it is interesting to note, but hardly surprising, that the one parameter where the error bars shrank considerably is for the outer eccentricity.

APPENDIX B: TABLES OF DETERMINED ECLIPSE TIMES FOR ALL SIX SYSTEMS

In this appendix, we tabulate the individual mid-minima times of the primary and secondary eclipses for the inner EBs of the triples considered in this study (Tables B1-B6).

The complete Appendix B is available in the on-line version of the journal, and also in the arXiv version; here we display only the first few lines of Table B1.

APPENDIX C: CLOSER LOOK AT THE DISTANCES

Here we attempt to compute the contribution to the uncertainty in *Gaia*'s parallax measurement due to the motion of the triple's centre of light ('col') as the stars move around in their orbits. Since all three stars are completely unresolved by *Gaia*'s optics, we consider only the motion of the centre of light around the triple's centre of mass. We treat the inner eclipsing binary as a single point source of light, and the tertiary as a second displaced light source in the system. The location of the centre of light is taken simply to be:

$$\vec{r}_{\rm col}(t) = \frac{\mathcal{R}_B(t)L_B - \mathcal{R}_A(t)L_A}{L_A + L_B}\,\hat{r} \tag{C1}$$

$$= \frac{(M_A L_B - M_B L_A)}{(M_A + M_B)(L_A + L_B)}\,\mathcal{R}(t)\hat{r} \tag{C2}$$

where $\mathcal{R}_B(t)$ and $\mathcal{R}_A(t)$ are the distances from the triple's centre of mass to the tertiary star (B) and binary (A, centre of mass), respectively, L_B and L_A are the luminosity of the tertiary and of the inner binary, respectively, and similarly for the masses M_B and M_A. For simplicity, here we consider only the bolometric luminosities. The vector $\hat{r}$ is the unit vector pointing from the system centre of mass to the tertiary star, and projected on to the plane of the sky. In turn, $\vec{\mathcal{R}}(t) \equiv \mathcal{R}(t)\hat{r}$ describes the ordinary Keplerian motion of the outer orbit of the triple system. The masses, luminosities, and orbital parameters are given in Tables 3, 4, and 5.

For each of our six triples, we used this prescription to compute the semi-major axis of the centre of light as it orbits the centre of mass of the triple system. To generate the motion on the sky as a function of time, we used the orbital parameters for the triples given in the Tables listed above. Because the orbits of all the triples are practically flat, and viewed nearly edge on, we simply took the motion to lie along a line on the sky. We do not know the position angle of the orbit projected on the plane of the sky, and so we used an illustrative angle of 45°, though after trying several different angles we realized the fact that our results are completely independent of this choice.

In Table C1 we give in columns 5, 6, and 7, the size of the semi-major axis of the centre of light in micro-arcseconds, the rms deviation from the parallactic ellipse that the orbit produces, and the error that this is likely to introduce into *Gaia*'s measurement of the parallax. For the latter we simply use the rms deviation divided by the square root of the number of measurements *Gaia* makes over

Table C1. Details of the Distance Determinations.

Target	Distance This work (pc)	Distance *Gaia* (pc)	π error[a] (μas)	a(col)[b] (μas)	rms(col)[c] (μas)	error(col)[d] (μas)	ϵ_i [e] (μas)	D [f] ...	RUWE[g] ...	Matched transits
37743815	1789 ± 78	1857 ± 39	11	119	104	15	35	1.20	1.09	54
42565581	3150 ± 150	3281 ± 160	15	63	47	11	39	1.04	1.17	24
54060695	2427 ± 34	2221 ± 50	10	80	57	7	37	2.26	0.94	67
178010808	1415 ± 22	1464 ± 30	13	90	73	10	56	5.14	1.04	59
242132789	2667 ± 28	3258 ± 165	16	73	52	9	32	0.82	1.10	37
456194776	1690 ± 24	1590 ± 40	16	159	130	20	52	4.46	0.95	49

Note. (a) *Gaia* uncertainty in the parallax (parallax_error). (b) Semimajor axis of the triple's centre of light ('col') expressed in micro-arc seconds. (c) RMS fluctuations due to the triple's centre of light motion. (d) Error contribution due to the triple's centre of light motion (see the text). (e) *Gaia*'s astrometric_excess_noise. (f) *Gaia*'s astrometric_excess_noise_significance. (g) *Gaia*'s renormalized unit weight error – RUWE parameter. (h) The number of astrometric_matched_transits.

the 34 month duration of the *Gaia* eDR3 data set minus the number of astrometric fitted parameters (6). The number of measurements is listed in the last column of Table C1 as astrometric_matched_transits. We note, though, that the exact value of the distance uncertainty introduced by the motion of the centre of light is also dependent on how the *Gaia* sampling (every few weeks) 'beats' up with the outer orbital period of the triple.[10]

The first four columns of Table C1 are the TIC number of the triple system, the distance determined in this work as part of the photodynamical solution, the distance determined by *Gaia*, and the cited uncertainty in *Gaia*'s parallax. Columns 8, 9, and 10 in Table C1 are several *Gaia* measures of how well the astrometric solution fits the observations. The parameter ϵ_i is the astrometric excess noise, which *Gaia* says 'measures the disagreement, expressed as an angle, between the observations of a source and the best-fitting standard astrometric model'. The parameter D is 'a dimensionless measure of the significance of the calculated astrometric_excess_noise (ϵ_i). A value $D \gtrsim 2$ indicates that the given (ϵ_i) is probably significant.' The parameter 'RUWE' is the 'renormalised unit weight error', and if large enough is sometimes taken as an indication that the source being observed consists of multiple stars. Finally, the last column gives the astrometric_matched_transits, i.e. the number of astrometric visits to the target.

From a perusal of Table C1, first we see that no value of RUWE substantially exceeds unity, indicating that the *Gaia* astrometric solution shows no real indication of stellar multiplicity. Second, for the three sources which show elevated values of D, indicating a somewhat significant value of the astrometric_excess_noise parameter, the *Gaia* distance and our distance differ by only 3–9 per cent out of $\sim$2 kpc. Finally, we see that the expected uncertainties introduced by the light centroid motions within the triple are typically factors of a few smaller than the cited astrometric_excess_noise and just comparable with the cited parallax error. Therefore, we conclude that the motions of the centre of light within the triple systems are just marginally at the level of affecting the distance measurements. However, all the evidence (see Table C1) suggests that the *Gaia* distances are not substantially affected by internal light centroid motions for our set of six sources.

The bottom line is that we generate our own independent distance measurements found as part of our photodynamical solutions. These are generally in fine agreement with those of *Gaia*, however, our claimed photometric distance uncertainties are smaller than those that *Gaia* reports, with no reason not to believe our photodynamic results.

Interestingly, a perusal of the column in Table C1 giving the rms motions of the centre of light in these systems shows that they are all in the range of 47–130 μas. These are eminently detectable as 'orbits' with *Gaia* in their future analyses.

[10]In this regard, for example, we note that the outer period of TIC 54060695 (60.8 d) is very close to 1/6 of a year.

[1]*Department of Physics, Kavli Institute for Astrophysics and Space Research, MIT, Cambridge, MA 02139, USA*
[2]*Baja Astronomical Observatory of University of Szeged, H-6500 Baja, Szegediút, Kt. 766, Hungary*
[3]*Konkoly Observatory, Research Centre for Astronomy and Earth Sciences, H-1121 Budapest, Konkoly Thege Miklósút 15-17, Hungary*
[4]*ELTE Eötvös Loránd University, Gothard Astrophysical Observatory, Szent Imre h. u. 112, 9700 Szombathely, Hungary*
[5]*MTA-ELTE Exoplanet Research Group, H-9700 Szombathely, Szent Imre h. u. 112, Hungary*
[6]*Amateur Astronomer, Glendale, AZ 85308, USA*
[7]*Amateur Astronomer, 12812 SE 69th Place Bellevue, WA 98006, USA*
[8]*NASA Goddard Space Flight Center, 8800 Greenbelt Road, Greenbelt, MD 20771, USA*
[9]*SETI Institute, 189 Bernardo Avenue, Suite 200, Mountain View, CA 94043, USA*
[10]*Citizen Scientist, c/o Zooniverse, Dept, of Physics, University of Oxford, Denys Wilkinson Building, Keble Road, Oxford OX1 3RH, UK*
[11]*Center for Astrophysics | Harvard & Smithsonian, 60 Garden St., Cambridge, MA 02138, USA*
[12]*Department of Experimental Physics, University of Szeged, 6720 Szeged, Dóm tér 9, Hungary*
[13]*Brorfelde Observatory, Observator Gyldenkernes Vej 7, DK-4340 Tølløse, Denmark*
[14]*National Space Institute, Technical University of Denmark, Elektrovej 327, DK-2800 Lyngby, Denmark*
[15]*Amateur Astronomer, 7507 52nd Place NE Marysville, WA 98270, USA*
[16]*Foundation for Scientific Advancement, Patterson Observatory, AZ 85650, USA*
[17]*Kavli Institute for Astrophysics and Space Research, MIT, Cambridge, MA 02139, USA*
[18]*Astronomical Institute, Slovak Academy of Sciences, 05960 Tatranská Lomnica, Slovakia*
[19]*Astronomical Institute, Charles University, Faculty of Mathematics and Physics, V Holešovičkách 2, CZ-180 00, Praha 8, Czech Republic*
[20]*Astrophysics Group, Keele University, Staffordshire ST5 5BG, UK*
[21]*Department of Physics and Astronomy, Michigan State University, East Lansing, MI 48824, USA*
[22]*Department of Astronomy & Astrophysics, The Pennsylvania State University, 525 Davey Lab, University Park, PA 16802, USA*
[23]*Center for Exoplanets and Habitable Worlds, The Pennsylvania State University, 525 Davey Lab, University Park, PA 16802, USA*

This paper has been typeset from a TEX/LATEX file prepared by the author.